4

Vehicle Dynamic Control of 4 In-Wheel-Motor Drived Electric Vehicle

Lu Xiong and Zhuoping Yu
Tongji University
China

1. Introduction

Thanks to the development of electric motors and batteries, the performance of EV is greatly improved in the past few years. The most distinct advantage of an EV is the quick and precise torque response of the electric motors. A further merit of a 4 in-wheel-motor drived electric vehicle (4WD EV) is that, the driving/braking torque of each wheel is independently adjustable due to small but powerful motors, which can be housed in vehicle wheel assemblies. Besides, important information including wheel angular velocity and torque can be achieved much easier by measuring the electric current passing through the motor. Based on these remarkable advantages, a couple of advanced motion controllers are developed, in order to improve the handling and stability of a 4WD EV.

2. Traction control

The fast and accurate torque generation of each driving wheel enables a great enhancement in traction control during acceleration.
In this section, an anti-slip controller for a 4WD EV using VSC (Variable Structure Control) method is presented. The control algorithm is independent on the identification of the road adhesion coefficient and has excellent robustness to the estimation error of the vehicle velocity. Regarding the high-frequency-chattering on the sliding surface, a new control method which combines the advantage of the VSC and MFC (Model Following Control) in order to decrease the fluctuation to the e-motor torque and slip ratio of the tire is proposed. The result of the simulation indicates that the proposed control method is effective for the ASR control and improves the performance of e-motor's output torque and the slip ratio of the tire.

2.1 VSC ASR controller

2.1.1 One-wheel-model

An accurate simulation model is important to verify the effect of the designed controller. Fig.2.1-1 shows a two degrees of freedom vehicle model. It only contains the vehicle's longitudinal motion and ignores air resistance and rotating resistance. Formula 2.1-1 shows the mathematical model:

$$M\dot{v}_x = F_d$$

$$I_w \dot{\omega} = T_m - F_x R \tag{2.1-1}$$

Here, M is the 1/4 vehicle mass, kg; v_x represents the longitudinal velocity, m/s; F_x is the driving force of the road, N; I_ω is the wheel rotational inertia, kg·m²; R is the wheel radius, m; ω is the angular velocity, rad/s and T_m is the motor torque, N·m.
The Magic Formula tire model is applied as the tire model, so the driving force F_d can be expressed as follows:

$$F_d = \mu_{Max} \cdot F_Z \cdot \sin\left(C \cdot \arctan\left\{B(1-E)\lambda + E \cdot \arctan(B\lambda)\right\}\right) \tag{2.1-2}$$

The meanings of the parameters can be found in the literature [1].

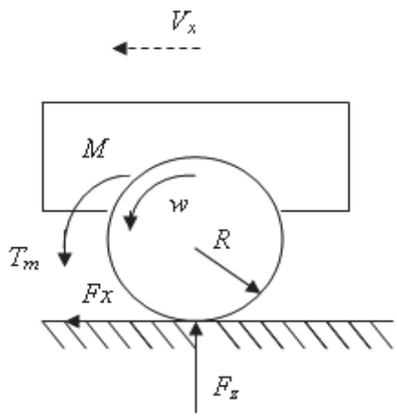

Fig. 2.1-1. One-wheel-Model

2.1.2 Design of VSC ASR controller

VSC with sliding mode has good robustness to the input signals so that this strategy has advantage to the ASR control system which needs the vehicle velocity observation and signal identification. But there is always high-frequency-chattering on the sliding surface. In the following text a VSC controller, which doesn't depend on the identification of the optimal slip ratio, is designed and its performance will be analyzed through simulation.
In order to make the VSC possess excellent robustness to the additional uncertainties and interferences, the control law adopted here is equivalent control with switching control. Hence, the output torque of the e-motors can be expressed as [2]:

$$T_m = T_{m,eq} - \Delta T \,\mathrm{sgn}(s) \tag{2.1-3}$$

In this equation, $T_{m,eq}$ is the equivalent torque of the e-motor, ΔT is the hitting control drive torque, sgn(s) is the switching function of the system.
The sliding motion includes two processes: approaching motion and sliding motion. The approaching motion can make the system at any time in any position approach to the sliding face in limited time. The sliding motion occurs only when the system reaches sliding surface:

$$s = \lambda - \lambda_{reference} = 0 \,.$$

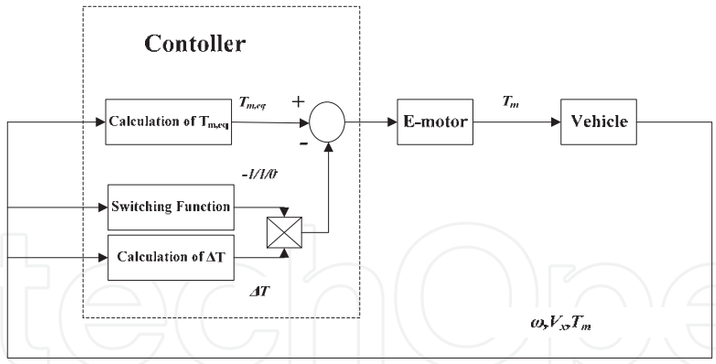

Fig. 2.1-2. Diagram of VSC ASR Strategy

To reach the ideal sliding mode, the requirement s=0 should be fulfilled. Assuming the reference slip is constant, so $\dot{\lambda}_{reference} = 0$
So, on the sliding face there is:

$$\dot{\lambda} = \dot{\lambda}_{reference} = 0 \tag{2.1-4}$$

According to the one-wheel model:

$$I_\omega \dot{\omega} = T_m - F_x R$$

During driving process, the slip ratio of the wheel can be expressed as:

$$\lambda = \frac{\omega R - v}{\omega R}$$

Combining Formula (2.1-1) and (2.1-4), we can get:

$$\frac{d\lambda}{dt} = -\frac{1}{\omega R}\left[\dot{v} - (1-\lambda)R\frac{T_m - F_x R}{I_\omega}\right] = 0$$

Then, we can obtain the e-motor's equivalent torque:

$$T_{m,eq} = \frac{I_\omega}{R(1-\lambda)}\dot{v} + F_x R$$

As the tire's longitudinal velocity is difficult to be measured accurately, $\hat{v}$ is the estimated value. Then the above formula can be rewritten as:

$$\hat{T}_{m,eq} = \frac{I_\omega}{R(1-\lambda)}\dot{\hat{v}} + F_x R \tag{2.1-5}$$

In the actual driving progress, there are many kinds of road surfaces and their respective optimal slip ratios. The identification for them is difficult. Through Fig. 2.1-3, we can see that, although the slip ratios for different roads are different, the basic shapes for μ-λ curves are

similar. It means, before the optimal slip ratio, the bigger the slip ratio, the larger the longitudinal adhesion coefficient is. While after the optimal slip ratio, the bigger the slip ratio, the smaller the longitudinal adhesion coefficient is[3].

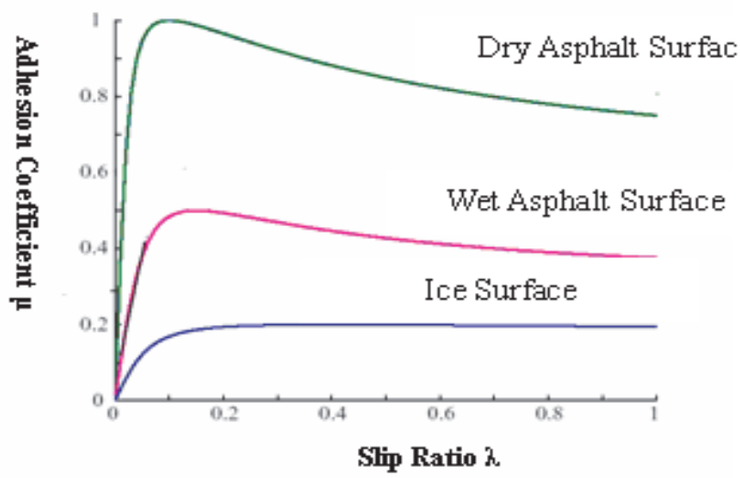

Fig. 2.1-3. Slip ratio-Longitudinal adhesion coefficient on different road surface

From Fig. 2.1-3, we can get:

When $\frac{\mathrm{d}\mu}{d\lambda} > 0$, $\lambda < \lambda_{reference}$, λ needs increasing so as to get larger adhesion coefficient and the driving torque should be increased.

When $\frac{\mathrm{d}\mu}{d\lambda} = 0$, $\lambda = \lambda_{reference}$, λ needs keeping so as to get larger adhesion coefficient and the driving torque should be maintained.

When $\frac{\mathrm{d}\mu}{d\lambda} < 0$, $\lambda > \lambda_{reference}$, λ needs decreasing so as to get larger adhesion coefficient and the driving torque should be reduced.

According to the one-wheel model, we can acquire: $\mu = \frac{T_m - I_\omega \dot{\omega}}{F_Z R}$

Then we can get:

$$\frac{d\mu}{d\lambda} = \frac{d\mu / dt}{d\lambda / dt} = \frac{\frac{\dot{T}_m - I_\omega \ddot{\omega}}{F_Z R}}{\frac{\dot{v}\omega R - v\dot{\omega}R}{(\omega R)^2}} = \frac{\omega^2}{F_Z} \cdot \frac{\dot{T}_m - I_\omega \ddot{\omega}}{\dot{v}\omega - v\dot{\omega}}$$

Now, we can get the judgment condition:

When $\frac{\dot{T}_m - I_\omega \ddot{\omega}}{\dot{v}\omega - v\dot{\omega}} > 0$, the e-motor's output torque needs increasing;

When $\frac{\dot{T}_m - I_\omega \ddot{\omega}}{\dot{v}\omega - v\dot{\omega}} = 0$, the e-motor's output torque needs keeping;

When $\frac{\dot{T}_m - I_\omega \ddot{\omega}}{\dot{v}\omega - v\dot{\omega}} < 0$, the e-motor's output torque needs decreasing.

From above we can find that what the switching function needs is not the slip ratio and the reference slip ratio any more, but the angular speed, e-motor's torque and driving torque, which need not identification. Although there is still longitudinal velocity estimation value in the controller, the controller itself has solved this problem which can be seen in Formula 8. So this VSC strategy is considered as feasible.

When the system is not on the sliding surface, it needs approaching the sliding surface from any state. This motion is called approaching motion. And during this motion the slip ratio will be approaching 0.

Under the generalized sliding condition, the switching function should meet:

$$s\dot{s} \le -\eta|s| \tag{2.1-6}$$

Here the parameter η >0. η represents the velocity, in which the system approaches the sliding surface. The larger the η is, the faster the approaching velocity is. Whereas, the chattering on the sliding surface will be bigger.

When Formula (2.1-1) is put into Formula (2.1-6), we can get:

$$-\frac{s}{\omega R}[\dot{v} - (1-\lambda)R\frac{\hat{T}_m - \Delta T\,\mathrm{sgn}(s) - F_x R}{I_\omega}] \le -\eta|s| \tag{2.1-7}$$

Here the hitting control driving torque is assumed as

$$\Delta T = \frac{\omega I_\omega}{(1-\lambda)}(F+\eta) \tag{2.1-8}$$

Putting Formula 2.1-7 into Formula 2.1-6, we can get:

$$\left|\frac{1}{\omega R}(\dot{v}_x - \hat{\dot{v}}_x)\right||s| \le F|s|$$

That is:

$$F \ge \frac{1}{\omega R}\left|\dot{v}_x - \hat{\dot{v}}_x\right| \tag{2.1-9}$$

So the e-motor's output torque can be shown as

$$T_m = \hat{T}_{m,eq} - \Delta T\,\mathrm{sgn}(s) \tag{2.1-10}$$

The simulation results for vehicle that starts on the road surface with a low adhesion coefficient（μ=0.2）is shown in Fig.2.1-4.

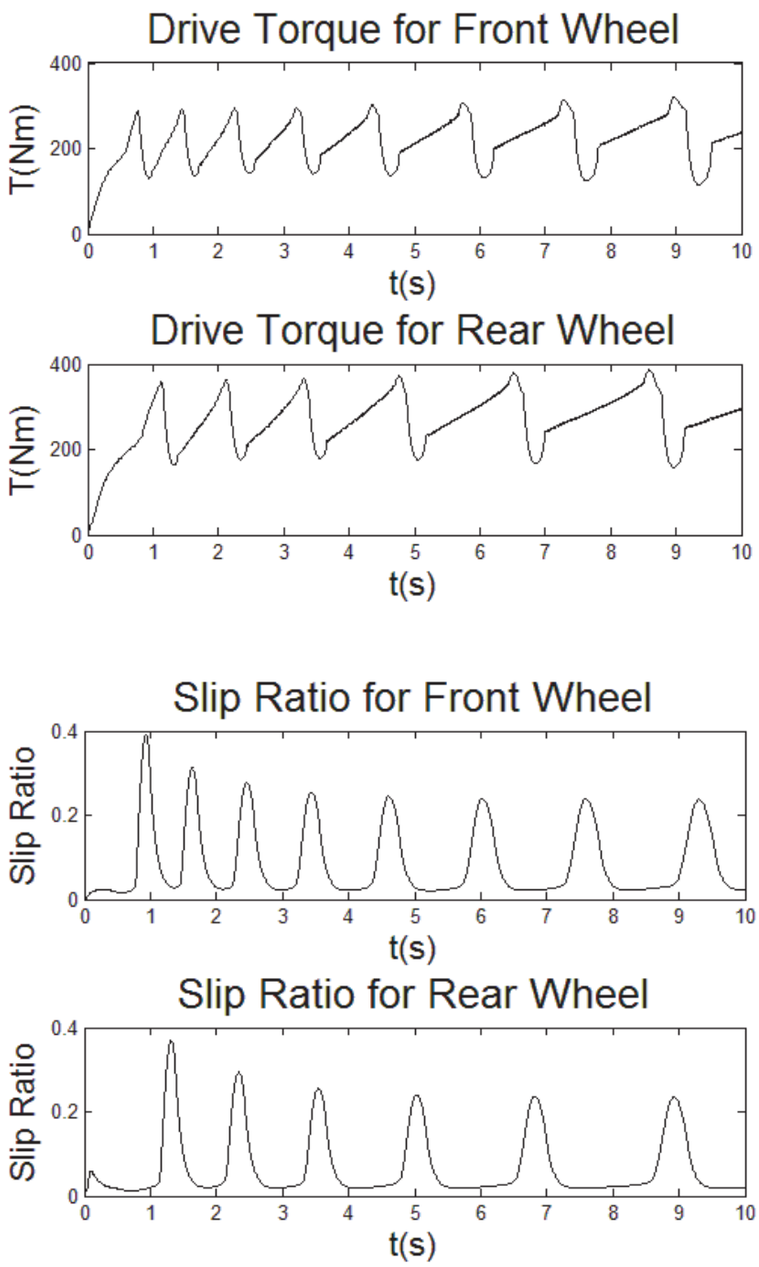

Fig. 2.1-4. Start on a low adhesion surface（μ=0.2）

From the simulation results we can get that the vehicle can keep away from skipping and the acceleration performance is good when it starts. But the slip ratio occurs fluctuation when it's among 0 to 0.3 and the e-motor's output torque also fluctuates near 300Nm. In reality, big fluctuation is harmful to the e-motor and sometimes the e-motor can't fully realize what the controller requires. Therefore, there are some defects in this method.

2.2 ASR combined controller

2.2.1 MFC controller

According to the research results from Tokyo University [4, 5], when the tire is completely adhered, the vehicle's equivalent mass is equal to the sum of the sprung mass and non-sprung mass. When the tire slips, the angular speed changes significantly. During acceleration, the angular speed is obviously smaller than the ideal value which is outputed by the standard model. In light of this principal, the tire's angular speed should be compared to the angular speed from the standard model at any time. And then the difference is used as the basis for a correction value through a simple proportional control to adjust the e-motor's output torque. So that the tire can avoid slipping.

MFC strategy only requires the e-motor's output driving torque and the tire's angular speed signal to put ASR into practice. Consequently the estimation of the longitudinal velocity and the optimal slip ratio identification can be ignored. Therefore, this strategy is practical. The system diagram is shown in Fig.2.2-1.

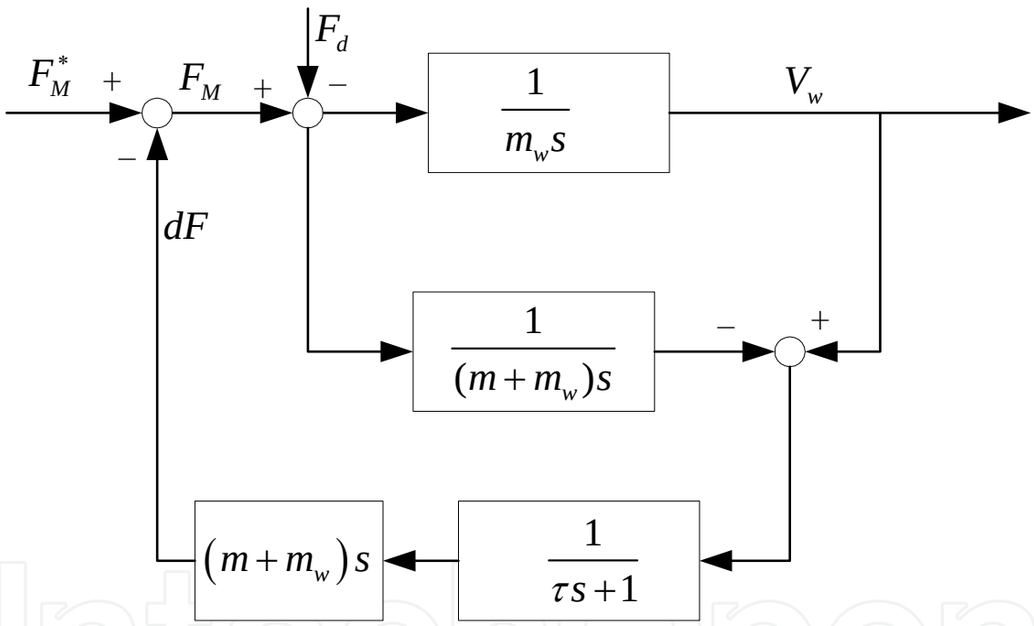

Fig. 2.2-1. MFC control block diagram

The standard model of MFC is got under the condition that the slip ratio is set to 0. It means that the road's adhesion force isn't fully utilized and the driving performance will be bad. So this control strategy is not perfect. Secondly, MFC hasn't good robustness to the input signals. Especially when the angular speed is disturbed, deviation of the controller will happen.

2.2.2 Combined controller

Based on the characters of VSC and MFC, in this section an area near the sliding surface will be set, within which the MFC strategy is applied. And out of this area, the VSC strategy is used.Thus, the high-frequency-chattering near the sliding surface can be avoided. The system diagram is shown in Fig.2.2-2 and Fig.2.2-3.

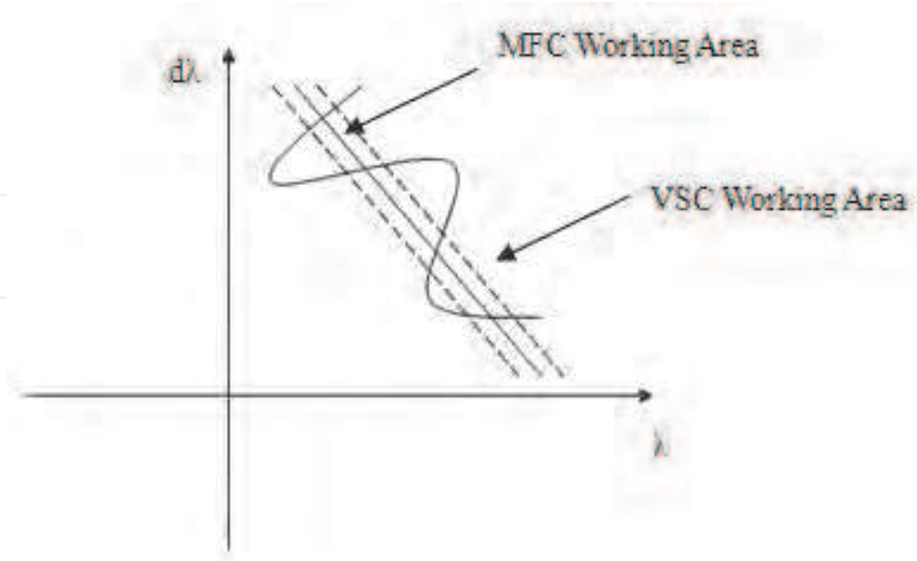

Fig. 2.2-2. Schematic diagram of switch region of combined control

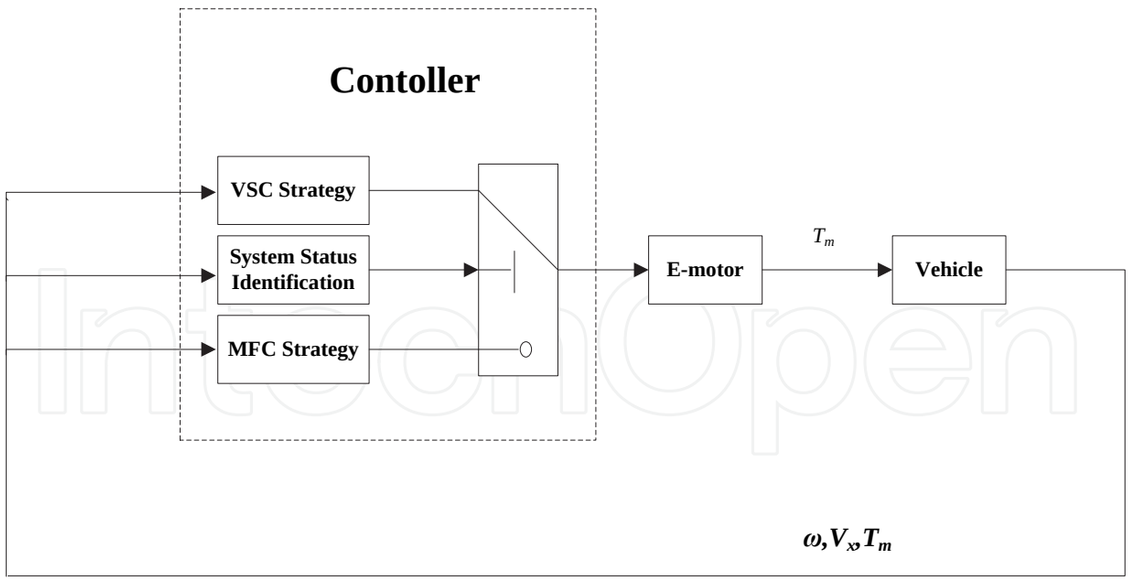

Fig. 2.2-3. Combined control block diagram

The simulation results for the vehicle that starts on the road surface with a low adhesion coefficient（μ=0.2） is shown in Fig.2.2-4.

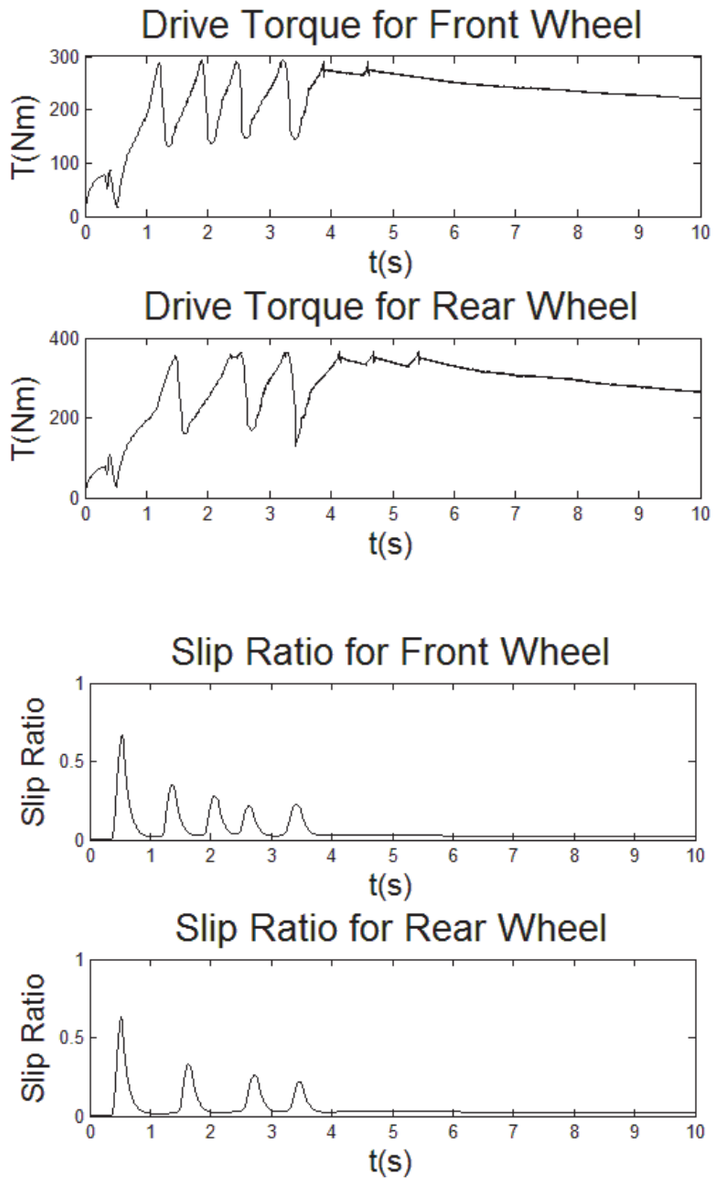

Fig. 2.2-4. Start on a low adhesion surface(μ=0.2)

From Fig.2.2-4, we can see that, on a low adhesion coefficient road surface, the vehicle doesn't slip. The slip ratio is in the ideal scope. Comparing with the above mentioned VSC strategy, the fluctuation of the slip ratio for combined control is improved. The fluctuation time continues 2.5s before stable convergence range occurs and the peak of the fluctuation of the slip ratio is 0.5. With the work of the combined control strategy the fluctuation scope is narrowed and the same to the e-motor's output torque. The drive performance for the combined control strategy is also excellent. On the low adhesion surface, the longitudinal velocity can reach 17m/s after 10s from starting.

Table 1 shows the driving performance for different control methods on road surface with low adhesion coefficient (μ=0.2).

	Drive distance(m)	Time(s)	Average acceleration(m/s2)	Utilization of adhesion coefficient
Without Control	36	7.5	1.33	68%
MFC	29	5.8	1.72	88%
Combined control	26	5.7	1.75	89%

Table 1. Accelerate to 10m / s on road surface with low adhesion coefficient from starting

Fig. 2.2-5 displays the simulation results on the jump μ road（from μ=0.2 toμ=0.7 ）. The tire doesn't slip on this kind of surface. It demonstrates that the combined control strategy is effective to such surface, too.

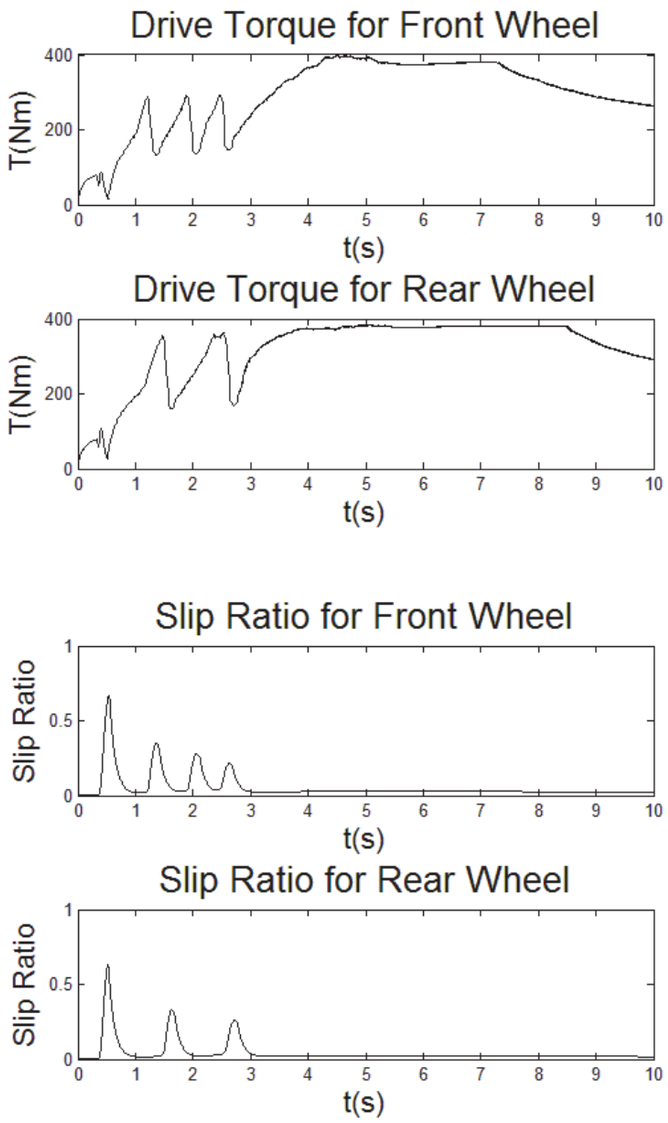

Fig. 2.2-5. Start on the jump μ road（from μ=0.2 toμ=0.7 ）

Fig.2.2-6 shows the simulation results with MFC strategy which is on the low adhesion coefficient road surface. In this simulation test, the wheel speed is disturbed that is manually offset by white noise(0.1kw) in order to verify the effectiveness to the disturb of the velocity signal.

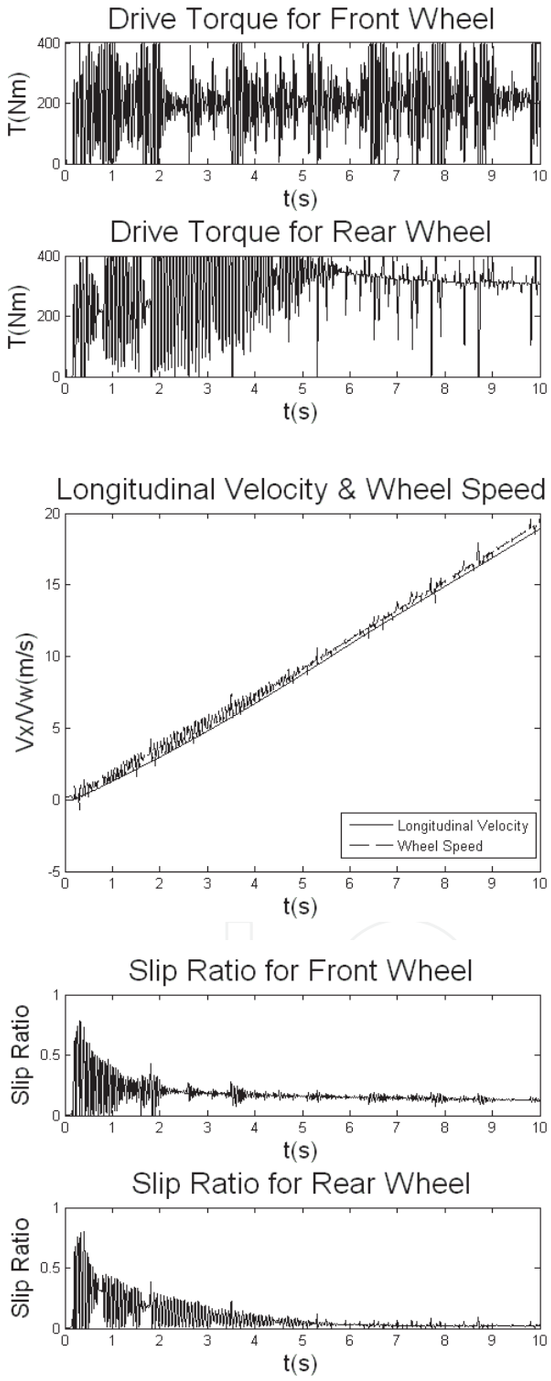

Fig. 2.2-6. Effectiveness to the disturb of the wheel speed signal for MFC control

From Fig.2.2-6, we can get that MFC has not good performance to the disturb of the wheel speed because the output drive torque is out of control. As we all known, the wheel speed is the only control parameter to this kind of strategy so that MFC control isn't regarded as an excellent control method to realize ASR function.

Fig.2.2-7 shows the simulation results on the low adhesion coefficient road surface which the longitudnal velocity is disturbed with combined control method. In this paper the longitudinal velocity is manually offset by a positive 2m/s and white noise. According to the results, the character of the combined control strategy is confirmed.

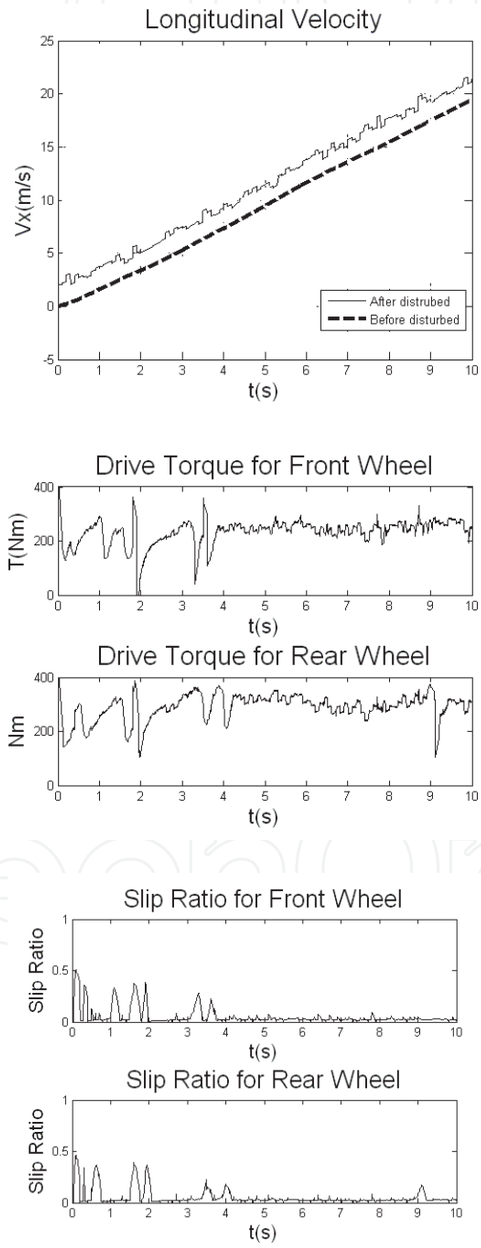

Fig. 2.2-7. Effectiveness to the disturb of the longitudinal velocity signal

According to results from Fig.2.2-6 and Fig.2.2-7, we can get that the combined control method has better robustness to the input signal's disturb. This point is very important to the usage of the control method.

3. Anti-lock brake control

For electric vehicles, the motor inside each wheel is able to provide braking torque during deceleration by working as a generator. Moreover, the torque response of an electric motor is much faster than that of a hydraulic system. Thanks to the synergy of electric and hydraulic brake system, the performance of the ABS (Anti-lock Brake System) on board is considerably improved.

In this section, a new anti-skidding method based on the model following control method is proposed. With the new feedback function and control parameter, the braking performance, especially the phase-delay of the electric motor's torque is, according to the result of the simulation, improved. Combined with the advantage of the origin MFC, the improved MFC can be widely applied in anti-skidding brake control.

Furthermore, a braking torque dynamic distributor based on the adjustable hybrid braking system is designed, so that the output torque can track the input torque accurately. Meanwhile a sliding mode controller is constructed, which doesn't perform with the slip ratio value as the main control parameter. Accordingly, the total torque is regulated in order to prevent the skidding of the wheel, so that the braking safety can be guaranteed.

3.1 Model following controller

3.1.1 One wheel model

When braking, slip ratio λ is generally given by,

$$\lambda = \frac{V_w - V}{V}$$

Where V is the vehicle longitudinal velocity and Vw is the wheel velocity. Vw=Rw, where R, w are the wheel radius and angular velocity respectively.

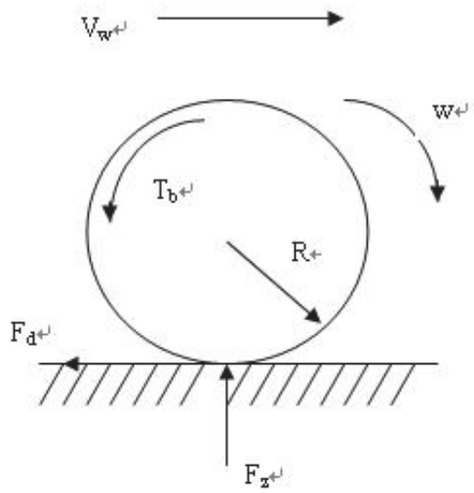

Fig. 3.1-1. One wheel model dynamic analysis

In the light of Fig. 3.1-1, the motion equations of one wheel model can be represented as

$$\mathrm{I_w}\frac{dw}{dt}=\frac{I_w}{R}\frac{dV_w}{dt}=F_d\cdot R-T_b \tag{3.1-1}$$

$$\mathrm{M}_w\frac{dV}{dt}=-F_d \tag{3.1-2}$$

In these equations, air resistance and rotating resistance are ignored. Mw is the weight of one wheel; I_W is the wheel rotational inertia; T_b is the braking torque, i.e. The sum of the hydraulic braking torque and the braking torque offered by the electric motor, and Fd is the braking force between the wheel and the road surface.

3.1.2 Design of MFC controller

The slip ratio is an important measurement for wheel's braking performance. For practical vehicle, it is difficult to survey this velocity. Therefore the slip ratio is hard to obtain. Compared with usual anti-skidding method, the method MFC(model following control) does not depend on the information-slip ratio. Consequently it is beneficial for the practical use.
According to the result by Tokyo University:

For the situation-skidding, the transmit function is $P(s)_{skid}=\frac{V_w}{F_{brake}}=-\frac{1}{M_w}\frac{1}{s}$

For the situation-adhesion, the transmit function is $P(s)_{adh}=\frac{V_w}{F_{brake}}=-\frac{1}{M/4+M_w}\frac{1}{s}$

The equation above is used as the nominal model in designing the controller "Model Following Controller". M represents the mass of the vehicle. Applying the controller, the dynamics of the going to be locked wheel becomes close to that of the adhesive wheel, through which the dynamics of the vehicle will be in the emergency situation.

3.1.3 Improved MFC controller

The above listed method, especially the feedback function is based on the one-wheel-model, but in fact there is always load-transfer for each wheel so that it cannot appropriately reflect the vehicle's state. According to the origin feedback function for one-wheel-model (M/4+Mw), which is introduced in the above-mentioned text, the information of the vertical load of each wheel can be used to substitute for (M/4+Mw). Here it is called equivalent mass and then the controller will automatically follow the state of the vehicle, especially for acceleration and deceleration situation.
The specific way to achieve this idea is to use each wheel's vertical load Fz to represent its equivalent weight. So the feedback function should be Fz/g instead of (M/4+Mw).When necessary, there should be a wave filter to obtain a better effect.
Another aspect ,which needs mo modify is its control parameter. For the method above, the control parameter is the wheel velocity Vw. In order to have a better improvement of the braking performance, the wheel angular acceleration $\frac{\mathrm{dw}}{dt}$ as the control parameter is taken advantage of.

Therefore the feedback function accordingly should be $\frac{R}{I_t+M/4*R^2}$.

With the idea of the equivalent mass, the feedback function should be $\frac{R}{I_t + F_z / g * R^2}$.

The reason why we take use of this control parameter is the electric motor itself also shows a delay (5~10ms) in an actual situation while the phase of the wheel angular acceleration $\frac{\mathrm{dw}}{dt}$ precedes that of the wheel velocity Vw. Consequently this control method can compensate the phases-delay of the electric motor.

3.1.4 Simulation and results

3.1.4.1 Simulation results with the wheel velocity as the control parameter

In the simulation, the peak road coefficient in the longitudinal direction is set to 0.2, which represents the low adhesive road. The top output torque of the electric motor is 136Nm and the delay time due to the physical characteristic of the electric motor 5 ms.

Fig. 3.1-2 shows the simulation result using the wheel velocity Vw as the control parameter. The braking distance is apparently decreased. The slip ratio is restrained under 20%. The unexpected increased amplitude of the slip ratio is mainly due to the delay of the electric motor's output, which can be proved in Fig. 3.1-2 (b). This can cause contradiction in the braking process. Fig. 3.1-2 (c) shows longitudinal vehicle velocity and wheel velocity under this control parameter.

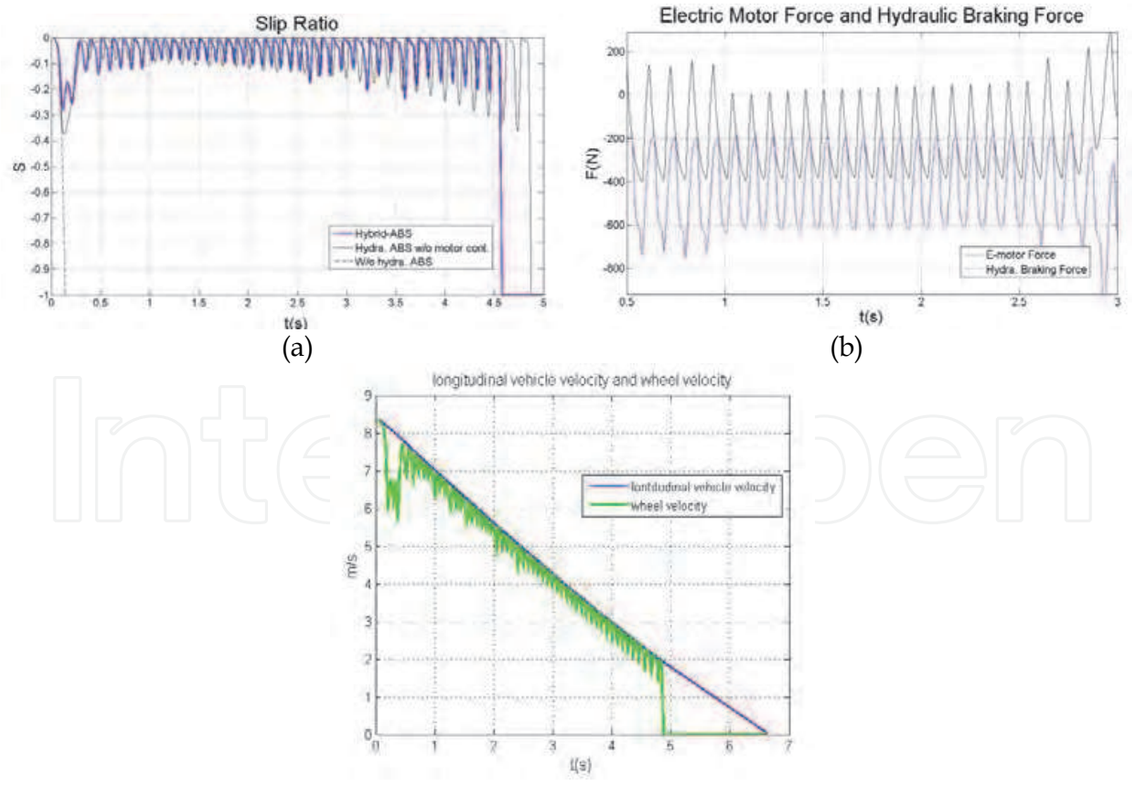

Fig. 3.1-2. Simulation Result of the Hybrid-ABS with the wheel velocity as the control parameter

3.1.4.2 The simulation results with the angular acceleration as the control parameter

Fig. 3.1-3 shows the simulation result using the wheel angular acceleration $\frac{dw}{dt}$ as the control parameter and increase the top output torque of the electric motor. Compared with the previous simulation result, it is clear that the braking distance is further shortened (compared with the system without electric motor control). The slip ratio is also restrained under 20% and is controlled better that the previous control algorithm. From Fig. 3.1-3 (b) we can see the phase-delay of the electric motor is greatly improved so that the two kinds of the torques can be simply coordinated regulated.

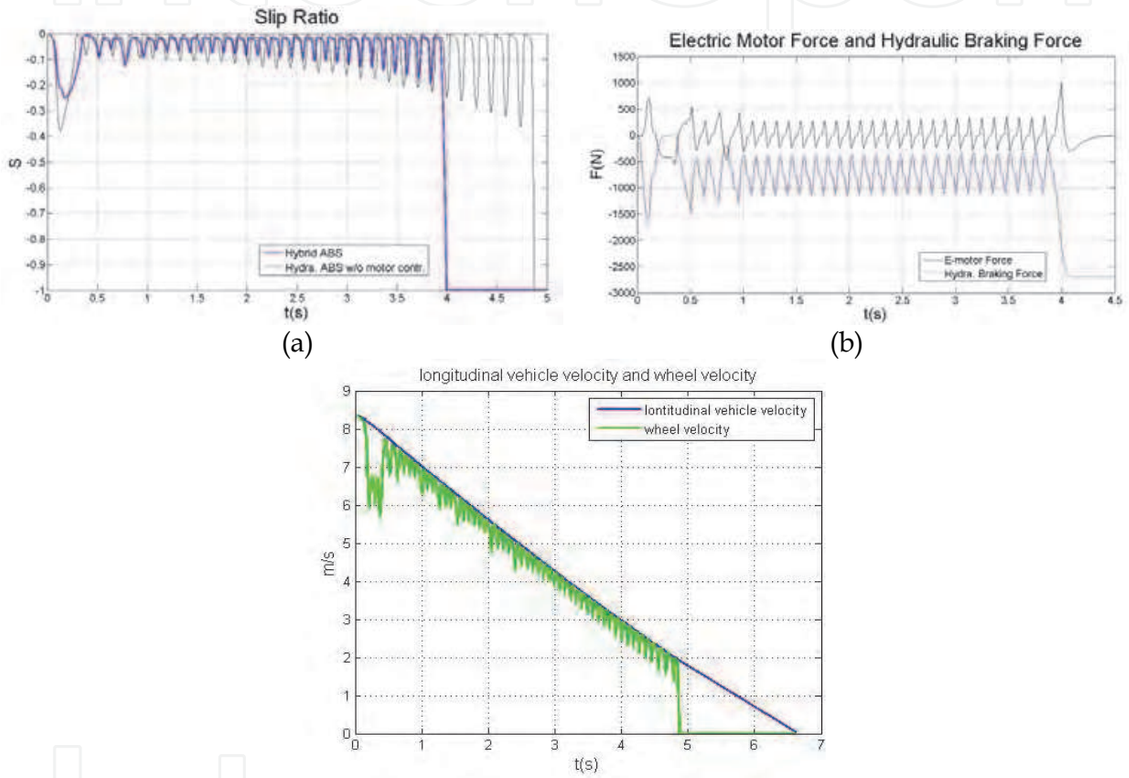

(a) (b)

(c)

Fig. 3.1-3. Simulation results of the Hybrid-ABS with the angular acceleration as the control parameter

Table 2 shows the result of the braking distance and the braking time under three above-mentioned methods.

	Hydraulic ABS without motor control	Hybrid ABS with MFC	Hybrid ABS with improved MFC
Braking distance(m)	27.9	26.8	26.5
Braking time(s)	5.12	4.87	4.83

Table 2. Results of the braking distance and the braking time under three different methods

3.1.5 Conclusion

According to the simulation results, the braking performance of the improved MFC is better than the performance of the origin MFC, proposed by Tokyo University. In future can we modify the MFC theory through the choice of the best slip ratio, because we know the value of the best slip ratio is not 0 but about 2.0. When we can rectify MFC theory in this aspect, the effect of the braking process will be better.

3.2 Design of the braking torque dynamic distributor

The distributor's basic design idea is to make the hydraulic system to take over the low frequency band of the target braking torque, and the motor to take over the high frequency band. Then the function of the rapid adjustment can be reached.

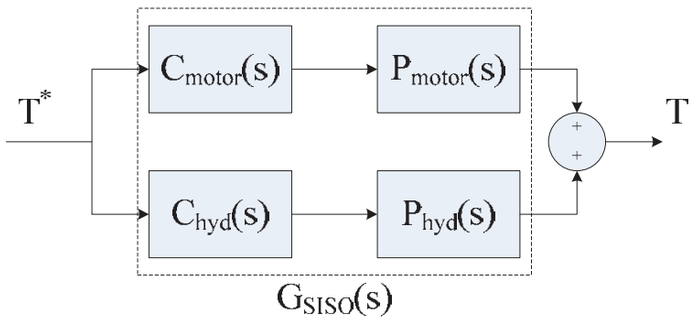

Fig. 3.2-1. The block diagram of the braking torque dynamic distributor

According to Fig. 3.2-1, C1(s) and C2(s) in Fig. 3.2-1 are the model of motor and hydraulic system. They can be written expressed as (1) and (2):

$$C_1(s) = \frac{1}{\tau_M s + 1} \tag{3.2-1}$$

$$C_2(s) = \frac{1}{\tau_H s + 1} \tag{3.2-2}$$

Here, τ_M and τ_H are time constants for motor and hydraulic system relatively.
In order to reach the goal to track the braking torque, $G_{SISO}(s) = 1$, that is,

$$C_1(s) \cdot G_1(s) + C_2(s) \cdot G_2(s) = 1 \tag{3.2-3}$$

We can put formula (3.2-1) and formula (3.2-2) into formula (3.2-3),

$$C_{motor}(s) \cdot \frac{1}{\tau_M s + 1} + C_{hyd}(s) \cdot \frac{1}{\tau_H s + 1} = \frac{1}{\tau s + 1} \tag{3.2-4}$$

$$\begin{aligned} C_{motor}(s) &= [\frac{1}{\tau s + 1} - C_{hyd}(s) \cdot \frac{1}{\tau_H s + 1}] \cdot (\tau_M s + 1) \\ &= \frac{\tau_M s + 1}{\tau s + 1} - C_{hyd}(s) \cdot \frac{\tau_M s + 1}{\tau_H s + 1} \end{aligned} \tag{3.2-5}$$

Here, τ is the sampling step
$C_{hyd}(s)$ is chosen as the second-order Butterworth filter, and then according to (3.2-5) we can get $C_{motor}(s)$. And the saturation torque of the motor is limited by the speed itself.

3.3 Design of the sliding mode controller

3.3.1 Design of switching function

The control target is to drive the slip ratio to the desired slip ratio. Here a switching function is defined as:

$$s = \lambda - \lambda_{reference} \tag{3.3-1}$$

The switching function is the basis to change the structure of the model. And the commonest way to change the structure is to use sign function- sgn(s). The control law here combines equivalent control with switching control so that the controller can have excellent robustness in face with the uncertainty and interference of the environment.
So the control law can be expressed as:

$$u = u_{eq} + u_{vss} \tag{3.3-2}$$

Therefore the braking torque can be represented as:

$$T_b = T_{b,eq} - \Delta T \,\mathrm{sgn}(s) \tag{3.3-3}$$

In practical engineering applications, the chattering may appear when sign function is used. Therefore the Saturation function 'sat ()' is used to substitute for sign function.

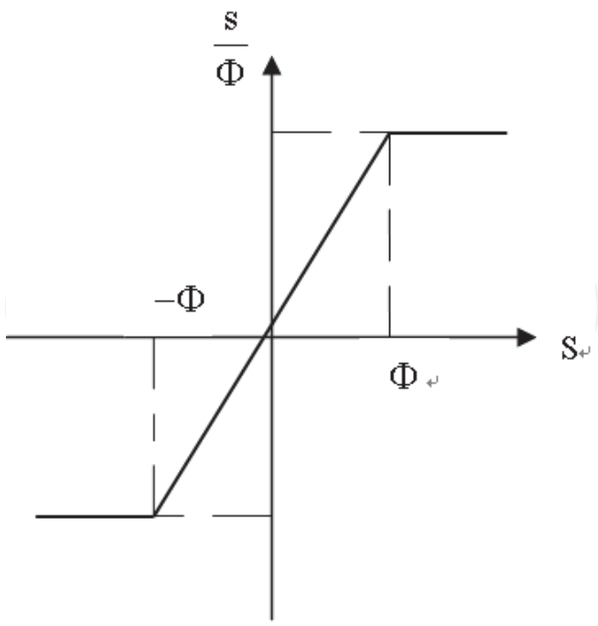

Fig. 3.3-1. Saturation function

So the braking torque can be expressed as:

$$T_b = T_{b,eq} - \Delta T sat(\frac{s}{\Phi}) \tag{3.3-4}$$

3.3.2 The improved sliding mode controller

One desired slip ratio can't achieve the best braking effect because of the inaccurate measurement of the vehicle speed and the change of the road surface. Then, a new method based on sliding mode control will be proposed according to the characteristic of the $\mu - \lambda$ curve. It can seek the optimal slip ratio automatically. The typical $\mu - \lambda$ curve is shown in Fig.3.3-2.

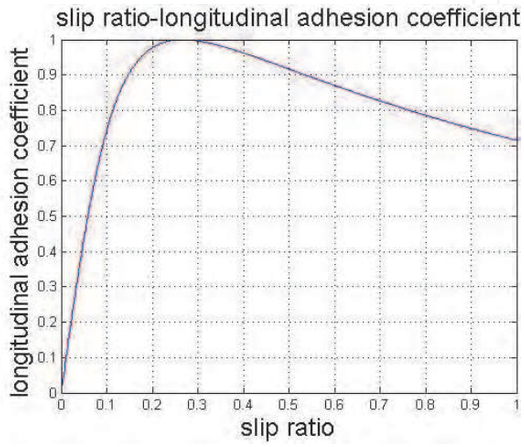

Fig. 3.3-2. $\mu - \lambda$ curve

From Fig. 3.3-2, we can see:

When $\frac{d\mu}{d\lambda} > 0$, $\lambda < \lambda_{reference}$, λ needs increasing in order to obtain larger μ. At this point we can increase the braking torque on the wheel;

When $\frac{d\mu}{d\lambda} = 0$, $\lambda = \lambda_{reference}$, λ needs maintaining in order to obtain larger μ. At this point we can maintain the braking torque on the wheel;

When $\frac{d\mu}{d\lambda} < 0$, $\lambda > \lambda_{reference}$, λ needs decreasing in order to obtain larger μ. At this point we can decrease the braking torque on the wheel.

According to the one wheel model and the definition of slip ratio, we can receive:

$$\frac{d\mu}{d\lambda} = \frac{d\mu / dt}{d\lambda / dt} = -\frac{\dot{T}_b + I_w \ddot{w}}{F_Z R} * \frac{V_x}{R\dot{w}} \tag{3.3-5}$$

$$= -\frac{\dot{T}_b + I_w \ddot{w}}{\dot{w}} * \frac{V_x}{F_Z R}$$

That is:

When $-\frac{\dot{T}_b + I_w \ddot{w}}{\dot{w}} > 0$, $\lambda < \lambda_{reference}$, $s = \lambda - \lambda_{reference} < 0$

When $-\frac{\dot{T}_b + I_w \ddot{w}}{\dot{w}} = 0$, $\lambda = \lambda_{reference}$, $s = \lambda - \lambda_{reference} = 0$

When $-\frac{\dot{T}_b + I_w \ddot{w}}{\dot{w}} < 0$, $\lambda > \lambda_{reference}$, $s = \lambda - \lambda_{reference} > 0$

The interval of the optimal slip ratio is commonly from 0.1 to 0.2. Therefore, when the slip ratio calculated by $\lambda = \frac{\omega R - V_x}{V_x}$ is larger than 0.3, we can judge that the current slip ratio is surely larger than the optimal slip ratio. The output of the sign function is 1.
So the algorithm based on $\mu - \lambda$ curve can be improved as:

When the slip ratio calculated by $\lambda = \frac{\omega R - V_x}{V_x}$ is bigger than 0.3, then we know that the actual slip ratio must be bigger than the optimal slip ratio, then the output of the sign function is 1;

When the slip ratio calculated by $\lambda = \frac{\omega R - V_x}{V_x}$ is smaller than 0.3,

i. If $|\dot{w}| > \phi_w$,

$$\begin{cases} \dfrac{J_w \ddot{\omega} + \dot{T}_b}{\dot{\omega} + \phi_w} > 0 & \text{sgn}(s) = 1 \\ \dfrac{J_w \ddot{\omega} + \dot{T}_b}{\dot{\omega} + \phi_w} < 0 & \text{sgn}(s) = -1 \end{cases}$$

ii. If $|\dot{w}| \le \phi_w$

Sign function maintains the output of the last step, that is: $\text{sgn}(s)_t = \text{sgn}(s)_{t-1}$.

3.3.3 Simulation and results

Fig. 3.3-3 shows the effect of the braking torque dynamic distributor. Since the existence of the saturation torque of the motor, it can't track the input torque when the input torque too large. When the demand torque is not too large, the braking torque dynamic distributor illustrates excellent capability.

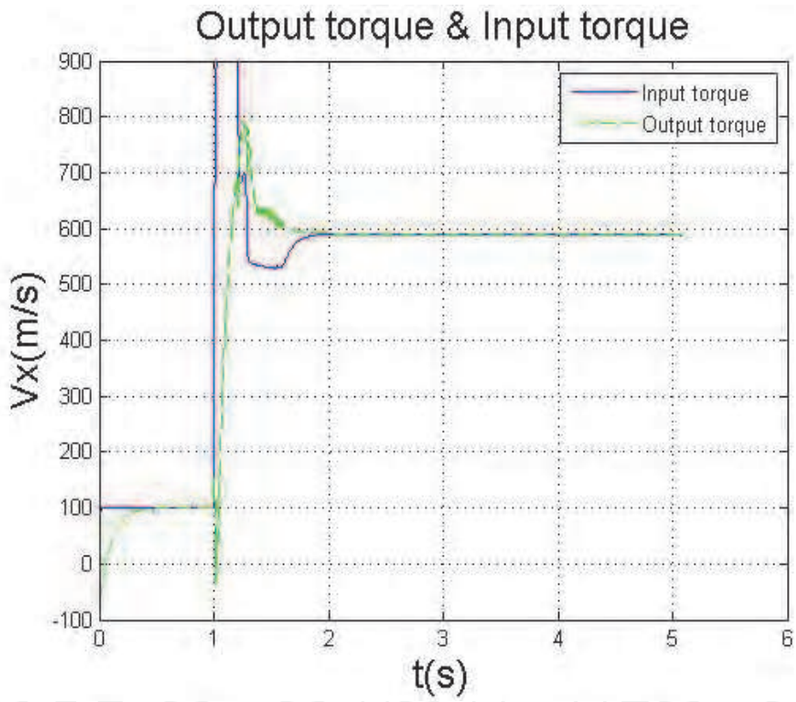

Fig. 3.3-3. The character of the braking torque dynamic distributor

Fig.3.3-4 - Fig.3.3-6 is the simulation results, which get from the improved sliding mode controller, and the initial velocity of the vehicle is 80km/h, the saturation torque of the motor is 180Nm：

i. When adhesion coefficient $\mu = 0.9$:

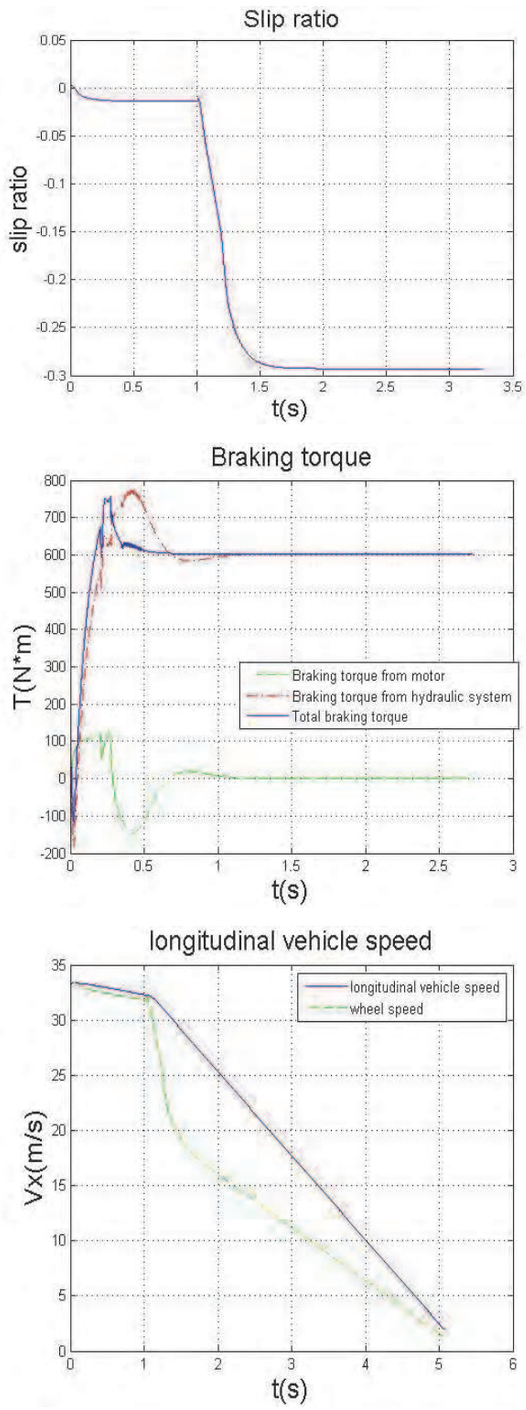

Fig. 3.3-4. Simulation results on the road with $\mu = 0.9$

ii. When adhesion coefficient $\mu = 0.2$:

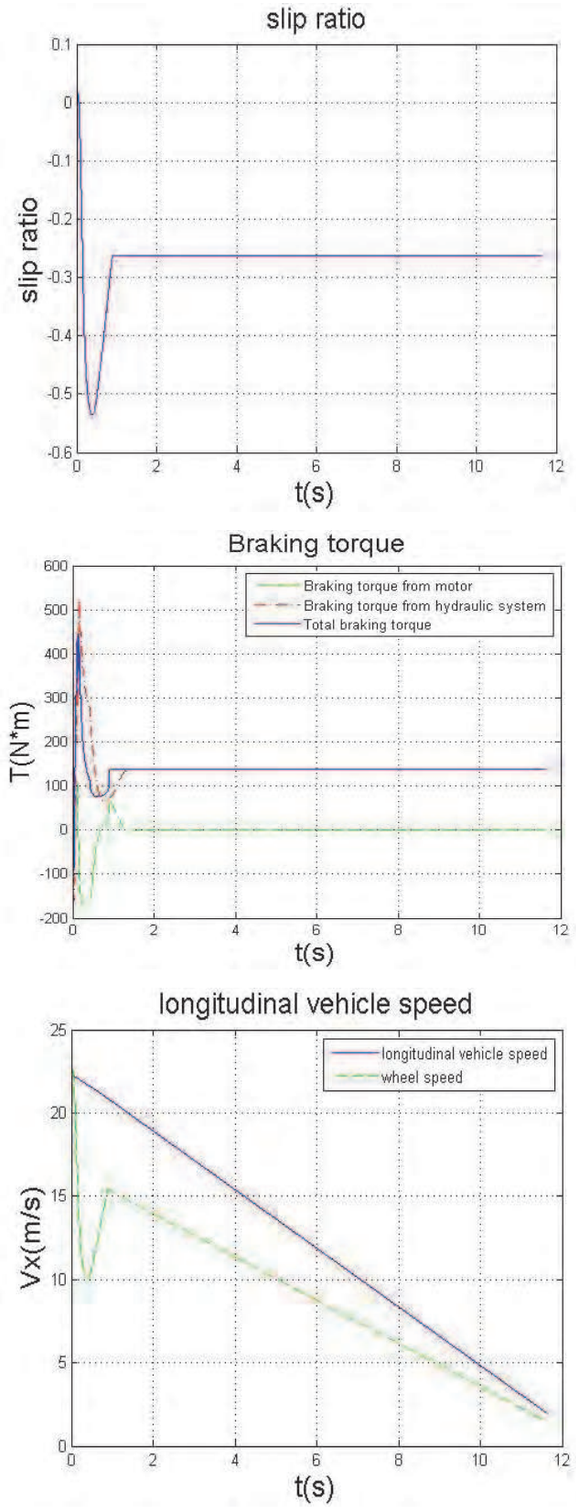

Fig. 3.3-5. Simulation results on the road with μ = 0.2

iii. When adhesion coefficient changes in 1st second from 0.2 to 0.9:

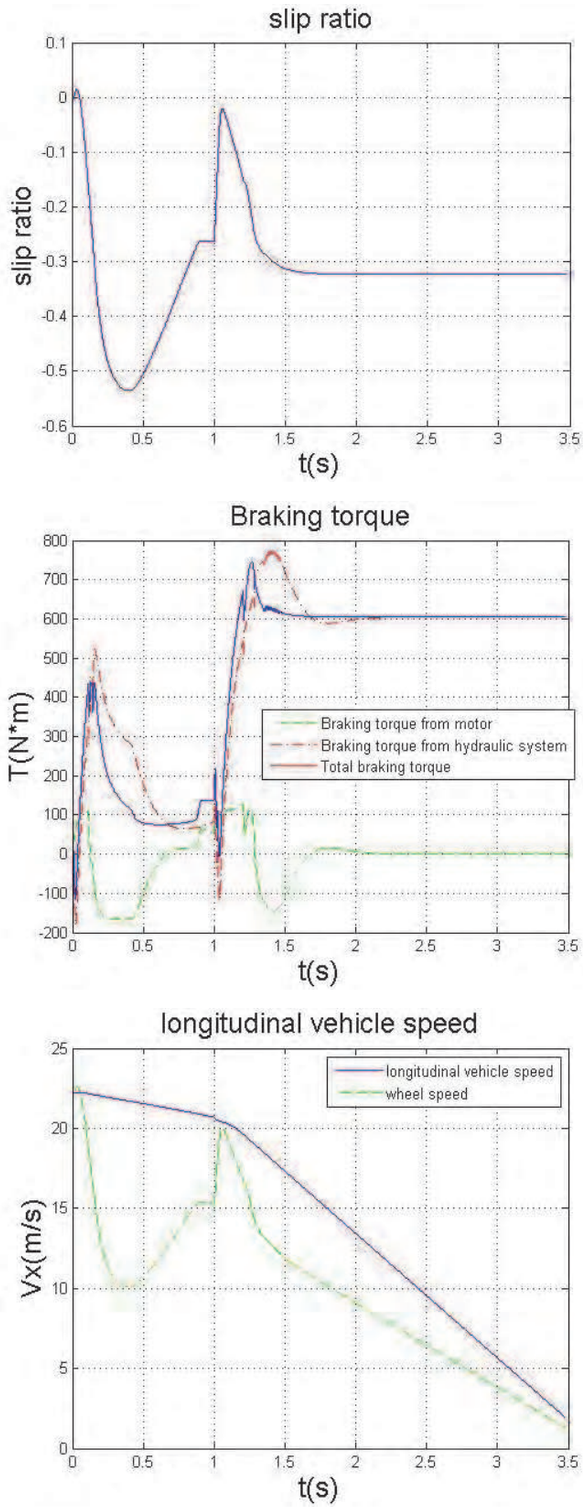

Fig. 3.3-6. The road adhesion coefficient changes from $\mu = 0.2$ to $\mu = 0.9$ at the 1st second

From Fig.3.3-4 -Fig.3.3-6, we know that, although this method doesn't regard slip rate as the main control information, this sliding mode can track the optimal slip ratio automatically. That means, both the longitudinal adhesion force and the lateral adhesion force can be made use of fully. Even on the road, whose adhesion coefficient increases suddenly, the controller can also find the optimal slip ratio.
During the braking process, the torque offered by the motor and hydraulic system doesn't oscillate distinctly. It indicates, the hybrid-braking system can achieve target braking torque actually.
Table 3 shows the braking distance and braking time on the different road. From the datum we know the braking safety can be guaranteed with this anti-skidding controller.

Number	Adhesion coefficient	Braking distance(m)	Braking time(s)
a)	0.9	33.99	2.71
b)	0.2	136.6	11.62
c)	0.2-0.9	50.23	3.47

Table 3. Braking distance and braking time on the different road

3.3.4 Conclusion

The braking torque dynamic distributor, which combines the merits of the two actuators motor and hydraulic system, can track the demanded torque promptly and effectively. The sliding mode controller has two sorts. One is to track the desired slip ratio, which is set manually and the effect of the controller good. However, the measurement of the vehicle velocity and the identification of the road limit the promotion of the usage. The other kind of controller can seek the optimal slip ratio automatically. Through the result of the simulation, the effectiveness of this controller is proved. It can have a wider range of application.

4. Vehicle stability control

Many researchers in the last decade have reported that direct yaw moment control is one of the most effective methods of active chassis control, which could considerably enhance the vehicle stability and controllability. The direct yaw moment control of a traditional ICE (Internal Combustion Engine) vehicle is based on the individual control of wheel braking force known as the differential braking. However, for EVs, the generation of desired yaw moment for stabilizing the vehicle under critical driving conditions can be achieved by rapid and precise traction/braking force control of each in-wheel-motor.
In this section, a hierarchical vehicle stability control strategy is introduced.
The high level of the control strategy is the vehicle motion control level. A dynamic control system of a 4 in-wheel-motored electric vehicle which improves the controlling stability under critical situation is presented. By providing the method of estimating the cornering stiffness and combining the controller with optimal control allocation algorithm, which takes account of the couple characteristic of the longitudinal/lateral force for tire under critical situation, the vehicle stability control system is designed. The double lane change simulation was carried out to verify the validity of the control method. Simulation result shows the proposed control method could stabilize the vehicle posture well under critical condition. Compared with the LQR with fixed cornering stiffness, the feedback from

identifying cornering stiffness to correct the parameters of the controller helps a lot in improving the robustness of the stability control.

The low level of the control strategy is the control allocation level, in which the longitudinal force's distribution is the focal point. Through the analysis of the tire characteristics under the combined longitudinal and lateral forces, an effectiveness matrix for the control allocation considering the longitudinal force's impact on the lateral force was proposed. Based on Quadratic Programming method the longitudinal forces on each wheel are optimal distributed. The simulation results indicate that the proposed method can enhance the vehicle handling stability, meanwhile the control efficiency is improved as well.

4.1 Vehicle dynamic control structure

Studies have shown that hierarchical control of the dynamics control method has a clear, modular control structure, as well as better control robustness, which is easy for real vehicle applications of the control algorithms. This hierarchical control architecture is widely adopted by general chassis's integrated control.VDC(vehicle dynamic control) introduces the hierarchical control structure, as shown in Fig. 4.1-1, the upper level is the vehicle motion control and the bottom level is the control allocation for each actuator.

The motion controller which belongs to the first level in the stability algorithm, collects the signals from the steering wheel's angle and the accelerator pedal, and calculates the generalized forces required by the stability control, including the longitudinal forces F_{xT} and yaw moment M_{zT}. The longitudinal forces can be directly calculated according to the accelerator pedal signals. The yaw moment can be got by following the reference model.

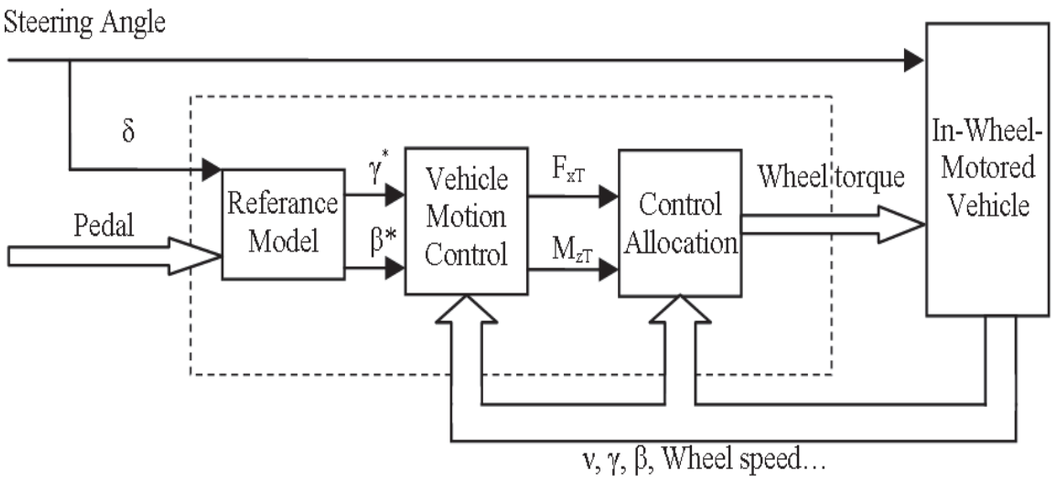

Fig. 4.1-1. Vehicle dynamic control structure

The control allocation is the second level of the vehicle controller. It is responsible to convert the "generalized forces" to the sub-forces on each actuator according to certain distribution rules and under some external constraint conditions (such as the maximum output of the motor and the road adhesion coefficient, etc.). And then to realize the optimum distribution of the each motor's torque. For a 4WD electric vehicle driven by 4 in-wheel-motors, the sub-force on each actuator is just the tire longitudinal force formed by the motor's output torque.

4.2 Vehicle motion controller

The yaw moment control is based on the MFC (model follow control) method. As reference model, the DYC model could keep slip angle zero for stability. The gain scheduling control algorithm can revise the parameters real-timely through the cornering stiffness identification to improve the adaptability of the algorithm to the environment and the change of the model parameters. The variable structure control (VSC) is applied to design control algorithm, for considering the strong robust characteristic during uncertainty. With proposed non-linear vehicle model, a precise gain value for switch function will be calculated, in order to reduce chattering effect.

4.2.1 Vehicle model

4.2.1.1 Linear vehicle model

The simplified linear two freedom model make the side slip angle and the yaw rate as its state variables. As the control input, the yaw moment M_{zT} is gained from the longitudinal force allocation by the motors according to the required moment, the function is:

$$m \cdot V(\frac{d\beta}{dt} + \gamma) = F_{yf} + F_{yr} \tag{4.2-1}$$

$$J_z \frac{d\gamma}{dt} = M_y + M_{zT} \tag{4.2-2}$$

The description of the state space is:

$$\dot{X} = AX + E\delta + Bu \tag{4.2-3}$$

Here： $x = [\beta \quad \gamma]^T$, $u = M_{zT}$

$$A = \begin{bmatrix} -\frac{2(C_f + C_r)}{mV} & -1 - \frac{2(C_f l_f - C_r l_r)}{mV^2} \\ -\frac{2(C_f l_f - C_r l_r)}{J_z} & -\frac{2(C_f l_f^2 + C_r l_r^2)}{J_z V} \end{bmatrix}$$

$$E = \begin{bmatrix} \frac{2C_f}{mV} \\ \frac{2C_f l_f}{J_z} \end{bmatrix}, B = \begin{bmatrix} 0 \\ \frac{1}{J_z} \end{bmatrix} \tag{4.2-4}$$

$M_y = F_{yf} l_f - F_{yr} l_r$ represents the yaw motion caused by the lateral force acting on each wheel, F_{yf} , F_{yr} are the total front/rear wheel lateral forces. Other parameters are shown in Fig.4.2-1.

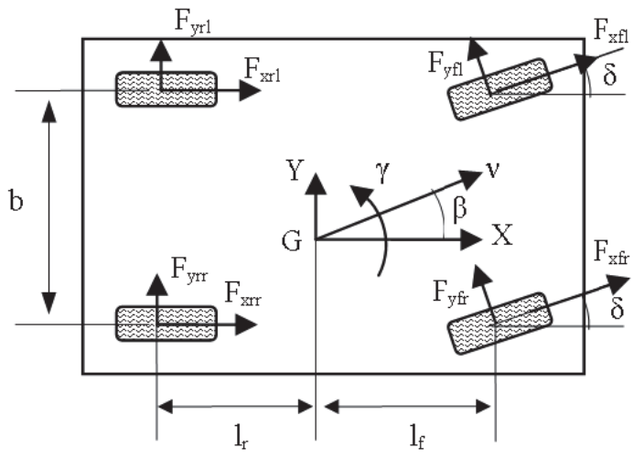

Fig. 4.2-1. Planar vehicle motion model

4.2.1.2 Non-linear vehicle model

In this paper the arc-tangent function is used to fit the lateral force formula, then a simple non-linear vehicle model can be obtained, the arc-tangent function contains two fitting parameters c_1, c_2, the fitting effect is show below:

The state space of One-track non-linear vehicle model can be express as: $\mathbf{x} = [x_1 \ \ x_2]^T = [\beta \ \ \dot{\psi}]^T, h_{(x)} = \beta = x_1$, β is the centroid-side angle of the vehicle, ψ is the course angle of the vehicle, u means additional yaw moment input M_{zT}, the complete function is:

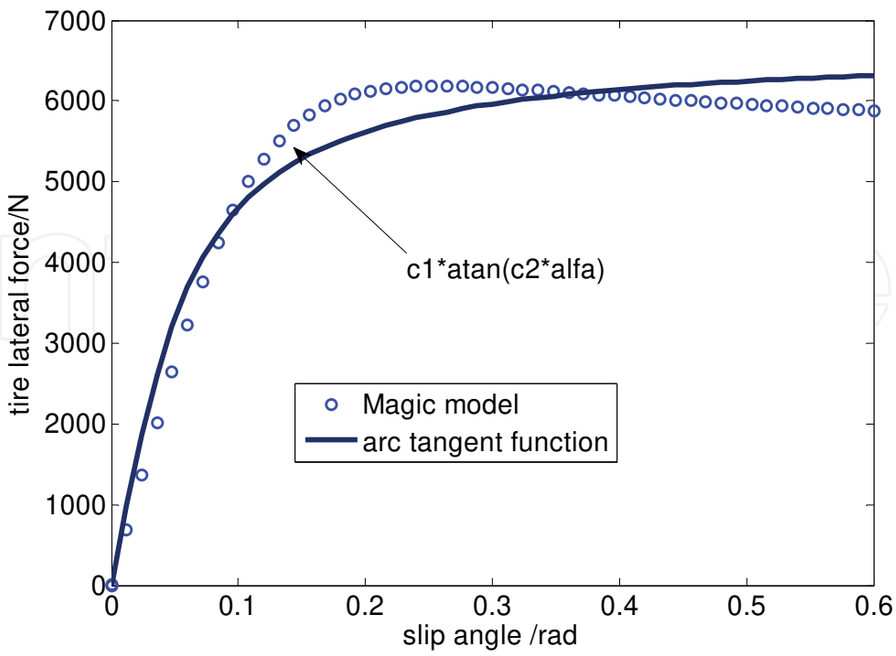

Fig. 4.2-2. Arc-tangent function vs. magic model

$$\begin{bmatrix}\dot{x}_1\\ \dot{x}_2\end{bmatrix}=\begin{cases}\frac{1}{mv}\{c_{f1}\,\mathrm{a\,tan}[c_{f2}(\delta_f-x_1-\frac{l_f}{V}x_2)]\cos\delta_f \\ \qquad +c_{r1}\,\mathrm{a\,tan}[c_{r2}(-x_1+\frac{l_r}{V}x_2)]\}-x_2 \\ \frac{1}{J_z}\{l_f c_{f1}\,\mathrm{a\,tan}[c_{f2}(\delta_f-x_1-\frac{l_f}{V}x_2)]\cos\delta_f \\ \qquad -l_r c_{r1}\,\mathrm{a\,tan}[c_{r2}(-x_1+\frac{l_r}{V}x_2)]+u\}\end{cases} \tag{4.2-5}$$

Here, m represents the mass of the vehicle, J_z represents the yaw rotational inertia of the vehicle, c_{f1} and c_{f2} are the fitting parameters for the front wheel, c_{r1} and c_{r2} are the fitting parameters for the rear wheel, l_f is the distance from the gravity point to the front axle and l_r is the distance from the gravity point to the rear axle, V is the gravity point velocity of the vehicle, δ_f is the steering angle for the front wheel.

Based on non-linear model mention above, we can design yaw-rate follow controller. In our case, the dynamic function of yaw rate is second-order system:

$$\begin{aligned}\ddot{\psi} &= f(X,t)+\Delta f(X,t)+g(u)+d(t)\\ &=\frac{1}{J_z}(F_{yf}(\alpha_f,F_{fz},\mu)\cdot l_f-F_{yr}(\alpha_r,F_{rz},\mu)\cdot l_r)\\ &\quad+\Delta f(X,t)+\frac{1}{J_z}u+d(t)\end{aligned} \tag{4.2-6}$$

Here, α_f is the side slip angle for the front wheel, α_r is the side slip angle for the rear wheel, F_{yf} and F_{yr} are the side slip force for the front and rear wheel, F_{fz} and F_{rz} are the vertical load for the front and rear wheel, μ is the road adhesion coefficient.

$f(X,t)$ indicates non-linear system function; $g(u)$ indicates non-linear continued function; $\Delta f(X,t)$ and $d(t)$ stand for uncertainty and external disturbance of controlled object, which are supposed to be zeros.

4.2.2 Reference model

The desired yaw-rate output is calculated from the reference model (DYC):

$$\dot{\gamma}_d=-\frac{1}{\tau_d}\cdot\gamma_d+\frac{k_d}{\tau_d}\delta \tag{4.2-7}$$

Here: $k_d=\dfrac{2C_fV}{mV^2+2(C_fl_f-C_rl_r)}$; $\tau_d=\dfrac{J_z\cdot V}{2(C_f{l_f}^2+C_r{l_r}^2)}$

4.2.3 Controller design

4.2.3.1 Gain scheduling controller

Based on the linear vehicle model, the controller adapts the LQR stability control algorithm. It is composed of feed-forward and feedback. Supposing the relationship between the feed-forward yaw moment and the front-wheel steering angle as:

$$M_{ff}(s) = G_{ff}\delta(s) \tag{4.2-8}$$

Here: G_{ff} is the feed-forward yaw moment coefficient. It can be calculated through the transfer function from vehicle side slip angle to front-wheel steering angle under stable condition, i.e. $\beta(s)/\delta(s)$ when $\beta(0) = 0$. Then.

$$G_{ff} = \frac{4C_f C_r l_f l_r - 2C_f l_f m V^2}{mV^2 + 2(C_f l_f - C_r l_r)} \tag{4.2-9}$$

Feedback control is used to decrease the control system's error caused by the unknown perturbation and the imprecise of the model, and to improve the reliability of the control system.

Define the state error $E = X - X_d$, from function (4.2-3), (4.2-7):

$$\dot{E} = AE + BM_{fb} + (A - A_d)X_d + (E - E_d)\delta \tag{4.2-10}$$

Considering the last two as perturbation, and according to LQR, assure the target function below to be least:

$$J = \int_0^\infty (EQE^T + uRu^T)dt \tag{4.2-11}$$

By solving the Riccati function，feedback coefficient G_{fb} is gained. And the feedback moment is:

$$M_{fb} = -G_{fb}E = -g_{fb1}(\beta - \beta_d) - g_{fb2}(\dot{\psi} - \dot{\psi}_d) \tag{4.2-12}$$

Total yaw moment required is:

$$M_{zT} = M_{ff} + M_{fb} \tag{4.2-13}$$

From the analysis above, we know the total yaw moment is decided by the feed-forward coefficient G_{ff} and feed-back coefficient G_{fb} together. And the coefficients can be adjusted on time according to the front and rear cornering stiffness identified and the vehicle speed measured. The control algorithm refers to the linear optimization calculation and on-line resolution of the Riccati function, which can affect the real time performance. On the real car the coefficients corresponding to different cornering stiffness and the vehicle speed are calculated off-line previously. Then a look-up table will be made from that and will be downloaded to the ECU for control. To easily show the movement of the feed-forward and feed-back coefficients, the following figure will illustrate the change of the front and rear cornering stiffness together through supposing the front cornering stiffness is changing, while the rear one is a fixed proportion to it.

Cornering stiffness is an important parameter for the controller. It will change along with the road condition or under the critical condition of the vehicle, which will further affect the control precise of the vehicle stability. The cornering stiffness that DYC control relies on is linear to the cornering stiffness under the current condition. So the cornering stiffness in this paper is estimated based on the two freedom linear model.

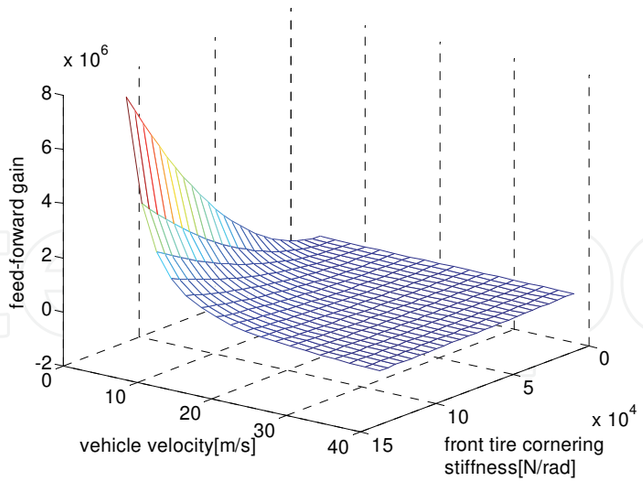

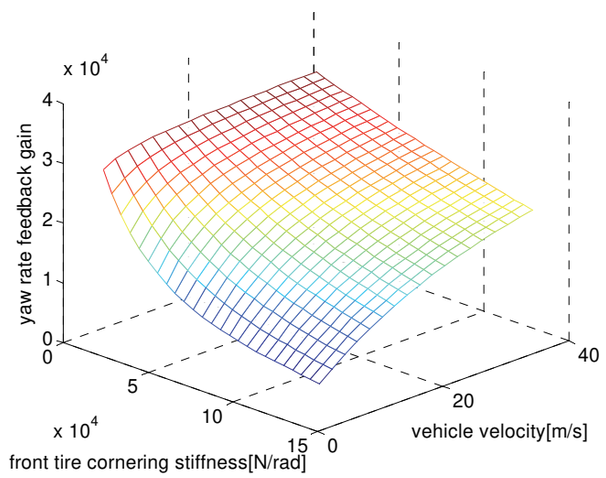

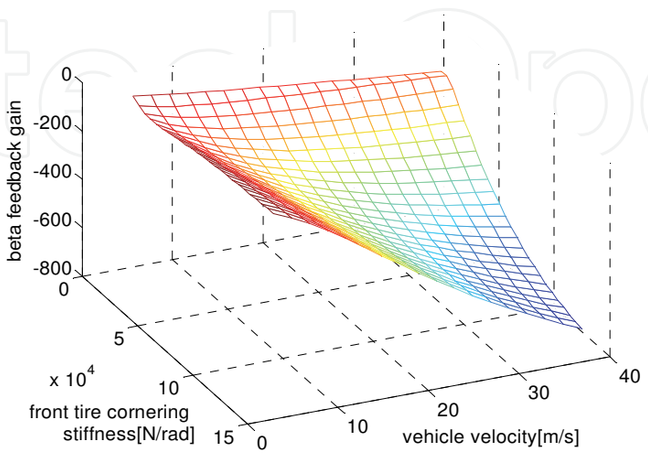

Fig. 4.2-3. Feed-forward/Feed-back Map

From function (4.2-2) , M_y is:

$$M_y = 2C_f(\beta + \frac{l_f}{V} - \delta)l_f - 2C_r(\beta - \frac{l_r}{V})l_r \tag{4.2-14}$$

Here C_f, C_r are front and rear nominal cornering stiffness. M_y above needs to be estimated by the yaw moment observation(YMO) below:

$$\hat{M}_y = F(s)(J_z\dot{\gamma} - M_{zT}) \tag{4.2-15}$$

Here: $F(s) = \omega_c / (s + \omega_c)$ is a filter function to gain $\dot{\gamma}$. ω_c is truncation frequency.
From function (4.2-14): to estimate the front and rear cornering stiffness separately, the estimator must provide the information of β . Therefore a united estimation of C_f, C_r, β needs to be established. To simplify the design, some change has been made to the function above. According to the magic tire model, the wheel cornering stiffness is pro rata to the load under a certain load range $(C_f l_f \approx C_r l_r)$. And as β is a small value, then:

$$C_f l_f \beta - C_r l_r \beta << M_y \ ; \tag{4.2-16}$$

Thus function (4.2-14) can be ：

$$M_y = -2C_f l_f (\frac{l_f + l_r}{V}\gamma - \delta) \tag{4.2-17}$$

$$\hat{M}_y(t) = \theta^T \cdot \varepsilon(t), \theta^T = C_f, \tag{4.2-18}$$

$$\varepsilon(t) = F(s) \cdot \left(-2l_f (\frac{l_f + l_r}{V}\gamma - \delta) \right) \tag{4.2-19}$$

Based on the above model, the front and rear cornering stiffness C_f, C_r will be gained by RLS estimation, as follows:

$$\hat{\theta}(k) = \hat{\theta}(k-1) - \frac{\Gamma(k-1)\varepsilon(k)}{\sigma + \varepsilon^T(k)\Gamma(k-1)\varepsilon(k)} \cdot \left\{ \varepsilon^T(k)\hat{\theta}(k-1) - y(k) \right\}$$

$$\Gamma(k) = \frac{1}{\sigma}\left\{ \Gamma(k-1) - \frac{\Gamma(k-1)\varepsilon(k)\varepsilon^T(k)\Gamma(k-1)}{\sigma + \varepsilon^T(k)\Gamma(k-1)\varepsilon(k)} \right\} \tag{4.2-20}$$

σ is forget factor and can be properly selected according to the road condition.
With the estimation result the controller parameters can be corrected on time. And a more precise general force can be gained to improve the allocation control of the vehicle.

4.3 Control alloction alogrithm

Through the control of the upper level, the yaw moment M_{zT} is gained, which will be allocated to each actuator to realize the control target (on 4WD EV is the motor torque).

4.3.1 Effectiveness matrix

Making approximation: $\sin\delta \approx 0$ and $\cos\delta \approx 1$, the total vehicle longitudinal force and the yaw moment caused by the longitudinal force are as follows:

$$\begin{aligned} F_{xT} &= F_{xfl} + F_{xfr} + F_{xrl} + F_{xrr} \\ M_{zxT} &= \frac{b}{2}(-F_{xfl} + F_{xfr} - F_{xrl} + F_{xrr}) \end{aligned} \tag{4.3-1}$$

Expressed as:

$$\begin{aligned} F_{xT} &= B_x \mathbf{F}_x \\ M_{zT} &= B_{zx} \mathbf{F}_x \end{aligned} \tag{4.3-2}$$

Where: $\mathbf{F}_x = [F_{xfl} \quad F_{xfr} \quad F_{xrl} \quad F_{xrr}]^T$; $B_x = [1 \quad 1 \quad 1 \quad 1]$, $B_{zx} = [-\frac{b}{2} \quad \frac{b}{2} \quad -\frac{b}{2} \quad \frac{b}{2}]$, B_x and B_{zx} are named as the effectiveness matrix.

In most researches, the vehicle yaw moment was directly obtained by (4.3-1). As the coupling characteristics of tires, the change of the tire longitudinal forces leads to the change of its' lateral force, especially in the critical conditions. So it's necessary to consider the additional yaw moment caused by the change of the lateral force.

Under certain tire sideslip angle α, the relationship between the four wheels' lateral and longitudinal forces can be expressed as:

$$\mathbf{F}_y = f_{yx}^{\alpha}(\mathbf{F}_x) \tag{4.3-3}$$

Where: $\mathbf{F}_y = [F_{yfl} \quad F_{yfr} \quad F_{yrl} \quad F_{yrr}]^T$

f_{yx}^{α} is a non-linear function, which brings complexity in the computation of the effectiveness matrix and the optimization of the control distribution. While if direct linear approximation was made to it, it would be too simplistic.

Discretization of the total yaw moment demand from the vehicle motion controller comes to:

$$M_{zT}(t+1) = M_{zT}(t) + \Delta M_{zT} \tag{4.3-4}$$

Supposing that δ is a small value, then $\sin\delta \approx 0$ and $\cos\delta \approx 1$. The increment of the total yaw moment can be expressed as:

$$\Delta M_{zT} = \mathrm{B}_{zx}\Delta\mathbf{F}_x + \mathrm{B}_{zy}\Delta\mathbf{F}_y \tag{4.3-5}$$

Here: $B_{zx} = \left[-\frac{b}{2} \quad \frac{b}{2} \quad -\frac{b}{2} \quad \frac{b}{2}\right]$, $B_{zy} = \left[l_f \quad l_f \quad -l_r \quad -l_r\right]$

$$\Delta\mathbf{F}_x = \begin{bmatrix} \Delta F_{xfl} & \Delta F_{xfr} & \Delta F_{xrl} & \Delta F_{xrr} \end{bmatrix}^T$$

$$\Delta\mathbf{F}_y = \begin{bmatrix} \Delta F_{yfl} & \Delta F_{yfr} & \Delta F_{yrl} & \Delta F_{yrr} \end{bmatrix}^T$$

Under a certain tire cornering angle α, the coupling relation of the tire longitudinal/lateral forces can be expressed as:

$$\mathbf{F}_y = f_{yx}^{\alpha}(\mathbf{F}_x) \tag{4.3-6}$$

Here: $\mathbf{F}_x = \begin{bmatrix} F_{xfl} & F_{xfr} & F_{xrl} & F_{xrr} \end{bmatrix}^T$, $\mathbf{F}_y = \begin{bmatrix} F_{yfl} & F_{yfr} & F_{yrl} & F_{yrr} \end{bmatrix}^T$.

then: $\Delta\mathbf{F}_y = \nabla f_{yx}^{\alpha}(\Delta\mathbf{F}_x)$

Magic formula can describe the tire characteristics under the combined working condition, but too complex. According to tire friction ellipse, the tire characteristics can be approximated expressed as: $\left(\frac{F_y}{F_{y0}^{\alpha}}\right)^2 + \left(\frac{F_x}{F_{x\max}^{\alpha}}\right)^2 = 1$, where F_{y0}^{α} is lateral tire force under tire sideslip angle α when longitudinal force equal zero, and $F_{x\max}^{\alpha}$ is maximum longitudinal tire force under tire sideslip angle α.

$$\left(\nabla f_{yx}^{\alpha}\right)_{ij} = \begin{cases} -\dfrac{{F_{y0i}^{i}}^2 \cdot F_{xi}}{F_{yi} \cdot {F_{x\max i}^{\alpha}}^2} & \text{i = j} \\ 0 & \text{i} \neq \text{j} \end{cases} \tag{4.3-7}$$

To substitute function (4.3-5) with (4.3-7), then:

$$\Delta M_z = (B_{zx} + B_{zy}\nabla f_{yx}^{\alpha})\Delta F_x \tag{4.3-8}$$

Then:

Set virtual control vector $v = \begin{bmatrix} \Delta F_{xT} & \Delta M_{zT} \end{bmatrix}^T$,

where the total longitudinal forces F_{xT} are created by the driver's pedal command. And the actual control vector $u = [\Delta F_{xfl} \quad \Delta F_{xfr} \quad \Delta F_{xrl} \quad \Delta F_{xrr}]^T$. Then the control allocation should meet the following equation:

$$v = B \cdot u \tag{4.3-9}$$

Where: the effectiveness matrix $B = \begin{bmatrix} B_x \\ B_{zx} + B_{zy}\nabla f_{yx}^{\alpha} \end{bmatrix}$

4.3.2 Optimal allocation algorithm

One objective of the control allocation can be expressed as to minimize the allocation error:

$$\begin{aligned} &\min \left\| W_v(Bu - v) \right\| \\ &s.t. \quad u^- \le u \le u^+ \end{aligned} \tag{4.3-10}$$

W_v is the weight matrix, reflecting the priority of each generalized force. The constraints include the limited capacity of the actuator, ie. the maximum torque range of in-wheel-motors, and the road adhesion ability.

At the same time, we also hope to minimize the energy consumption of the actuator.

Considering the characteristics of the tire adhesion, different wheels with different vertical load F_z , then the longitudinal forces and the lateral forces provided by each wheel are not the same. So the weight matrix W_u is introduced. It is a diagonal matrix, and the diagonal elements are:

$$w_{ii} = \frac{1}{\sqrt{(\mu_{ii} F_{zii})^2 - (F_{xii}^2 + F_{yii}^2)}} \tag{4.3-11}$$

Where μ is the road adhesion coefficient of each wheel. F_x , F_y and F_z are the longitudinal force, the lateral force and the vertical load of each wheel of the time.

Then another objective can be expressed as:

$$\begin{aligned} &\min \left\| W_u(u - u_d) \right\| \\ &s.t. \quad u^- \le u \le u^+ \end{aligned} \tag{4.3-12}$$

W_u considerate the characteristic of each tire adhesion, because different wheel is with different vertical load F_z .

The above (4.3-10) and (4.3-12) can be combined as followed Quadratic Programming (QP) problem:

$$u = \arg \min_{u^- \le u \le u^+} (\left\| W_u(u - u_d) \right\|_2^2 + \lambda \left\| W_\upsilon(Bu - \upsilon) \right\|_2^2) \tag{4.3-13}$$

Thus the computation time can be reduced largely. The parameter λ is usually set to very large in order to minimize the allocation error. The optimization problem can be solved through active set methods.

4.4 Simulation results and analysis

Using vehicle dynamics analysis software veDYNA, combined with the proposed vehicle stability control algorithm above, the high velocity double lane change operation is simulated to verify the validity of the control algorithm.

The vehicle is to carry out double lane change operation with the velocity of about 100km/h, which should be as constant as possible during the operation. Fig.4.4-2 shows the contrast between the vehicle trajectories with and without stability control. The vehicle could keep a steady posture and avoid obviously lateral slippage. Meanwhile compared to the LQR control without identification of the cornering stiffness, the algorithm designed in this paper can decrease the impact of the change of the model's parameters on the control effect. In addition a little under steering during lane change presents the steering characteristic of DYC reference model to restrain over large side slip angle.

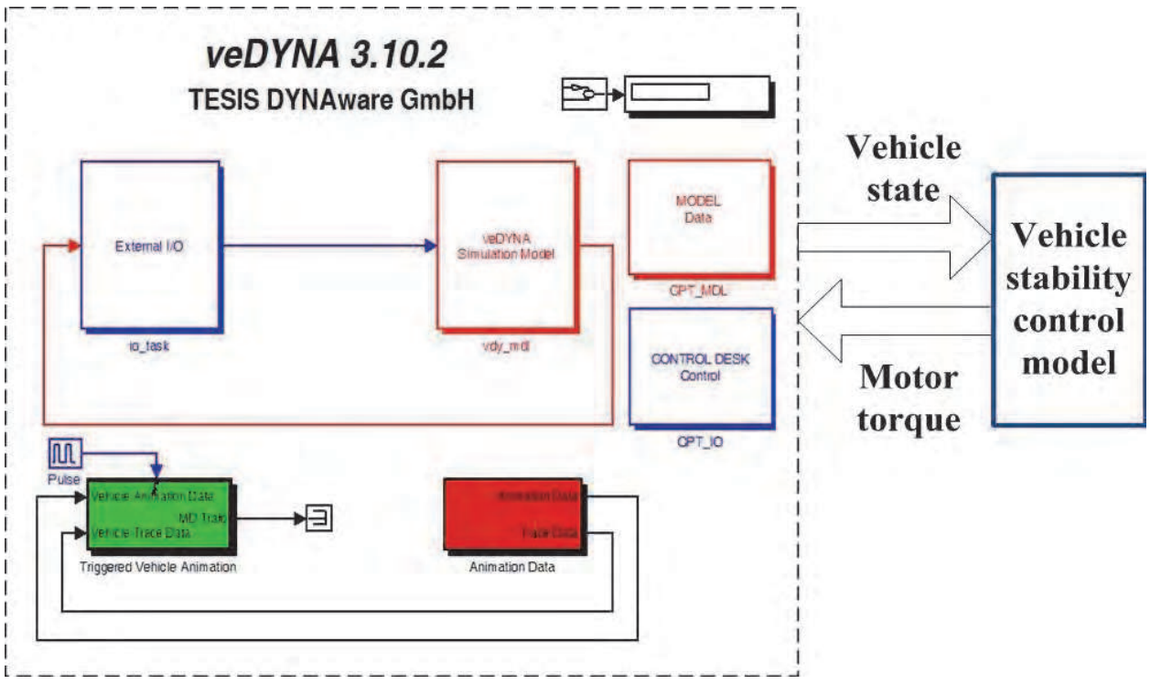

Fig. 4.4-1. veDYNA Simulation Model

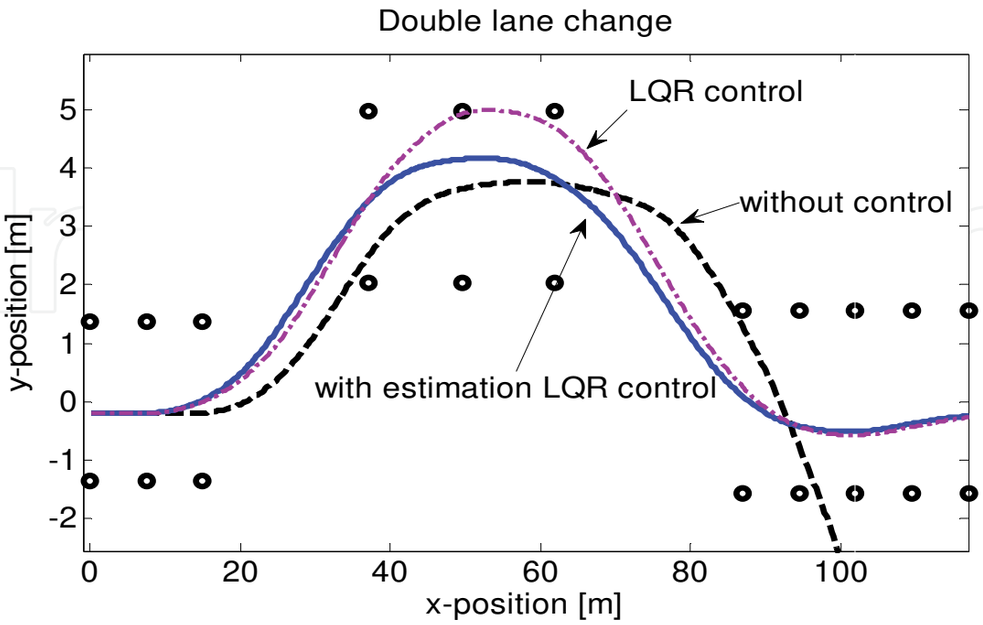

Fig. 4.4-2. Vehicle Trajectory

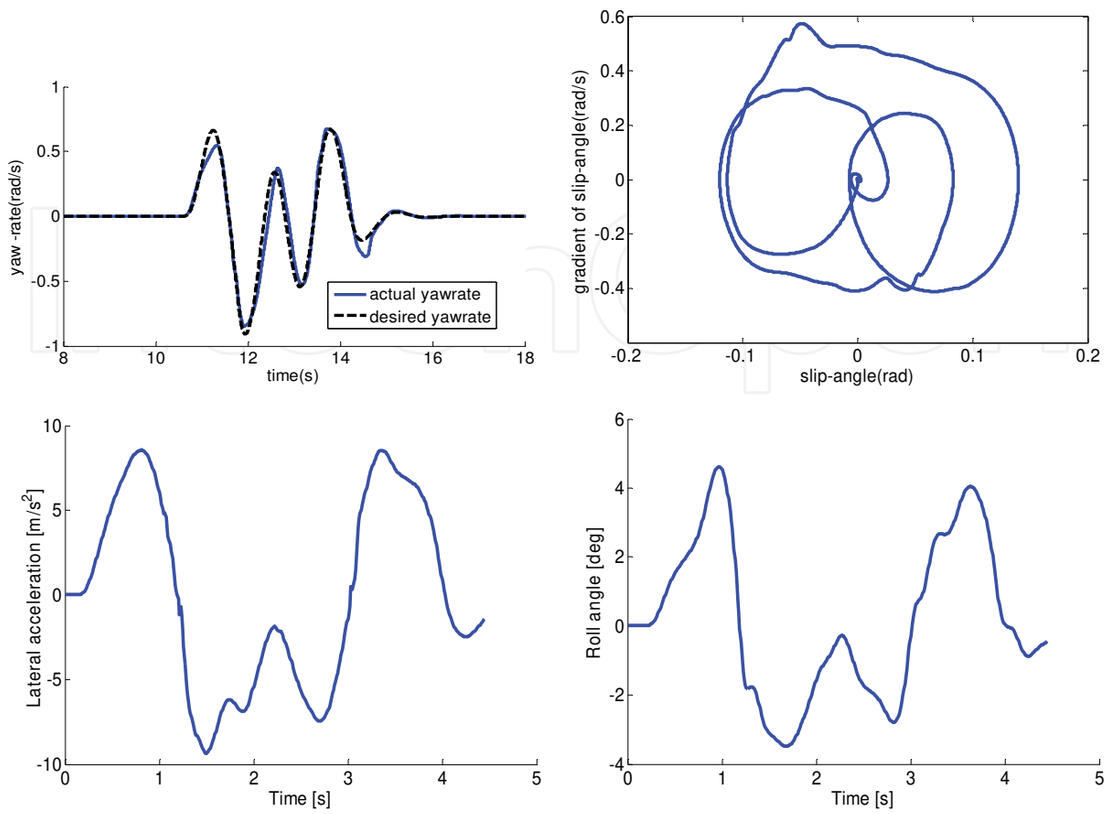

Fig. 4.4-3. Vehicle States

Fig. 4.4-3 presents the behaviors of several state values of the vehicle during such operation. Among them the yaw rate response can match the desired value well. Supposing on level and smooth road, when the peak value of the lateral acceleration is close to 1.0g, the vehicle has been working under critical condition. The $\beta - \dot{\beta}$ phase trajectory indicates that the vehicle can keep steady even when the slip angle reaches 8 degree.

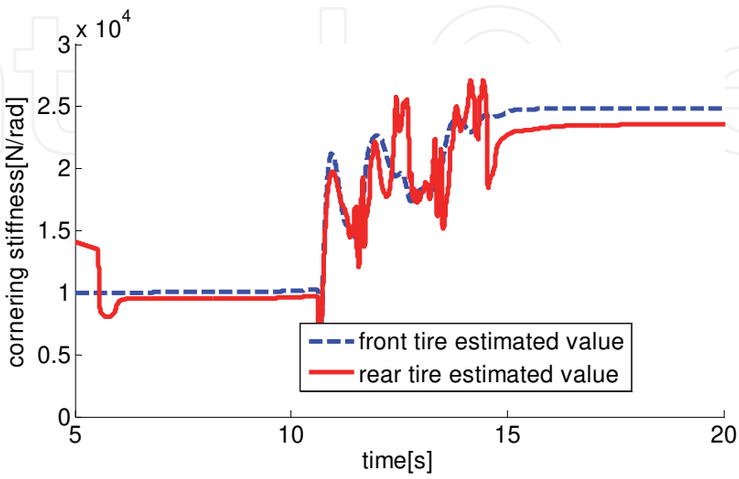

Fig. 4.4-4. Estimated Cornering Stiffness of Tire

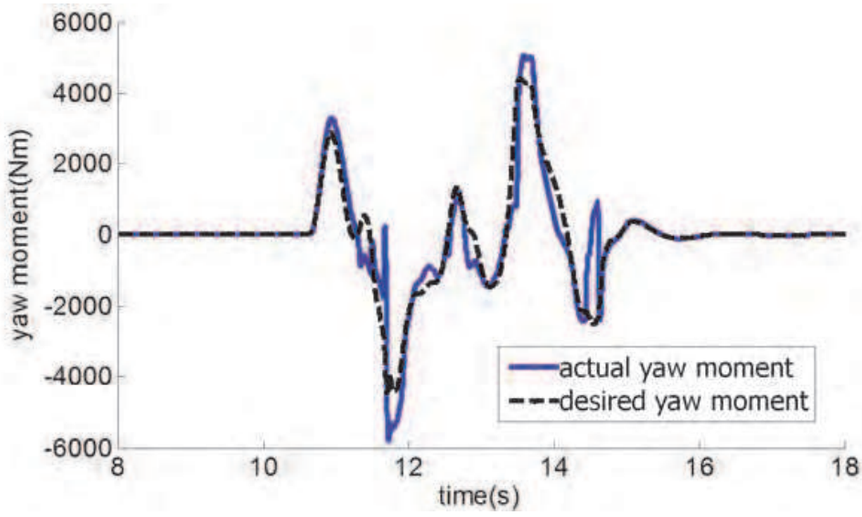

Fig. 4.4-5. Actual vs Desired Yaw Moment

Fig. 4.4-4 shows the estimated values of the cornering stiffness in the double lane change simulation, the vehicle lateral motion characteristic adjusts acutely during lane change. If the LQR controller were designed according to the fixed value of the cornering stiffness, the control effect would get worse along with the fluctuation of the cornering stiffness. Fig. 4.4-5 illustrates how the actual yaw moment follows the requirement of the control during the whole control process. It's clear that the optimize allocation algorithm can finely meet the requirement of the stability control even under the critical condition.

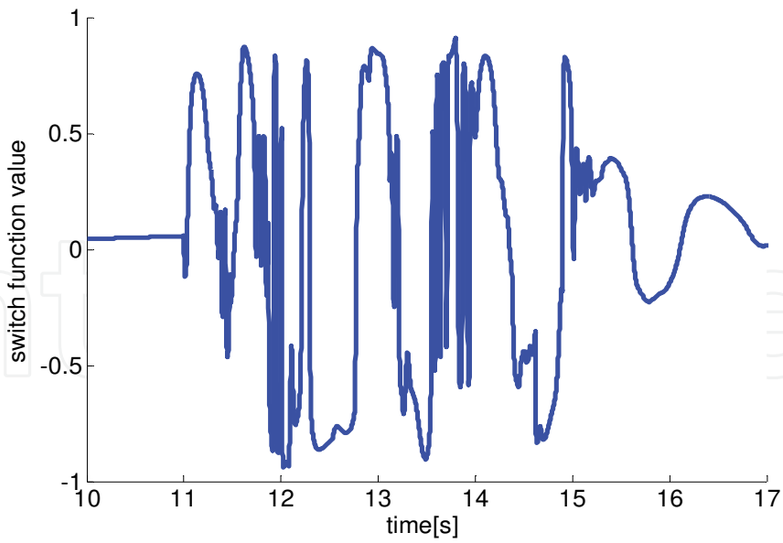

Fig. 4.4-6. Switch function value

Figure shows the adjustment of switch function value during operation; there is obvious chattering when simulation time is near 12s and 14s, but that causes no severe fluctuate to general yaw moment. Figure illustrates the actual yaw moment can realize the general control requirement basically, which guarantees the achievement of motion follow control.

4.5 Conclusion

In this section, a motion follow controller is designed based on the linear optimal control theory with the real time identification of the cornering stiffness and VSC theory with non-linear vehicle model. Considering the longitudinal/lateral forces' couple characteristic of tire under critical condition, the optimal control allocation algorithm realized the vehicle stability control successfully. Using veDYNA software, the double lane change simulation is carried out to verify the validity of the control method above.

The results of the simulation show: the proposed control method could stabilize the vehicle posture well under critical condition (i.e. the peak lateral acceleration is close to 1.0g and the slip angle reaches 8 degree). The reference model plays an important role on restraining the vehicle from losing stability. Compared with the LQR with fixed cornering stiffness, the feedback from identifying cornering stiffness to correct the parameters of the controller helps a lot in improving the robustness of the stability control. Actual control allocation could match the general requirement well by taking into account of tire force characteristic.

5. References

[1] D. Foito, A. Roque, J. Esteves, J. Maia, Electric Vehicle with two Independent Wheel Drives-Improving the Performance with A Traction Control System, Proceedings on the "17th International Electric Vehicle Symposium & Exposition - EVS 17", Montreal, Canada, October 2000.

[2] Buckholtz K R. Reference Input Wheel Slip Tracking Using Sliding Mode Control [R]. SAE 2002 World Congress, 2002.

[3] Zhaoliang Zhang, Lu Xiong and Zhuoping Yu. The Anti-skidding Control for Combined- braking System based on theadjustable Hydraulic System. 2010 IEEE International Conference on VehicularElectronics and Safety, Qingdao, 2010.

[4] Yoichi HORI，Future Vehicle driven by Electricity and Control -Research on Four Wheel Motored "UOT Electric March II", IEEE, Vol 51, 2004 P954 – 962.

[5] Shin-ichiro Sakai，Takahiro Okano, Tai Chien Hwa， 4 Wheel Motored Vehicle "UOT Electric March II" -Experimental EV for Novel Motion Control Studies-, Proc. of INTERMAC2001 Joint Technical Conference, Tokyo, Japan, 2001.

[6] Yoichi Hori, Yasushi Tyoda, and Yoshimasa Tsuruoka. Traction Control of Electric Vehicle: Basic Experimental Results Using the Test EV "UOT Electric March". IEEE Transactions on Industry Applications, vol.34, pp.1131-1137, September/October 1998.

[7] Buckholtz K R. Reference Input Wheel Slip Tracking Using Sliding Mode Control [R]. SAE 2002 World Congress, 2002.

[8] Y.Chamaillard, G.L. Gissinger, J.M.Perronne and M.Renner. An original braking controller with torque sensor. Proceedings of the Third IEEE Conference on Control Applications, 1994.

[9] A.El Hadri, J. C. Cadiou, K. N.M'Sirdi and Y. Delanne. Wheel-slip regulation based on sliding mode approach. SAE 2001 World Congress, 2001.UC Berkeley, November 1993.

[10] Kachroo P. Nonlinear Control Strategies and Vehicle Traction Control [D]. Ph.D .dissertation

[11] Shino,M.,Wang,Y.,Nagai,M., Motion Control of Electric Vehicle Considering Vehicle Stability. Proc.of AVEC2000,2000, pp.705-711
[12] Motoki Shino, Masao Nagai, "Yaw moment control of electric vehicle for improving handling and stability", JSAE Review 2001, pp.473-480
[13] Peng He and Yoichi Hori, "Optimum Traction Force Distribution for Stability Improvement of 4WD EV in Critical Driving Condition", 9thIEEE International Advanced Motion Control, Workshop, Istanbul, 2006
[14] Zhuoping Yu, Wei Jiang and Lijun Zhang, "Torque distribution control for four wheel in-wheel-motor electric vehicle", Tongji Daxue Xuebao/Journal of Tongji University, Vol. 36, No. 8, 2008, pp.1115-1119
[15] Sakai,S.,Hori,Y., Advanced Vehicle Motion Control of Electric Vehicle Based on The Fast Motor Torque Response. Proc.of AVEC2000, 2000 ,pp .729-736
[16] Chumsamutr,R., Fujioka,T., Improvement of Electric Vehicle's Cornering Performance by Direct Yaw Moment Control. Proc. of AVEC2000, 2000, pp.729-736
[17] H .Fujimoto, N .Takahashi, A. Tsumasaka and T. Noguchi. motion control of electric vehicle based on cornering stiffness estimation with yaw-moment observer. IEEE Int. Workshop Advanced Motion Control, 2006,pp. 206-211
[18] Peng He and Yoichi Hori, "Optimum Traction Force Distribution for Stability Improvement of 4WD EV in Critical Driving Condition", 9th IEEE International Advanced Motion Control, Workshop, Istanbul, 2006
[19] Zhuoping Yu, Wei Jiang and Lijun Zhang, "Torque distribution control for four wheel in-wheel-motor electric vehicle", Tongji Daxue Xuebao/Journal of Tongji University, Vol. 36, No. 8, 2008, pp.1115-1119
[20] H.B.Pacejka, "Tyre and Vehicle Dynamics", Butterworth Heinemann, 2002
[21] Brad Schofield and Tore Haegglund, "Optimal Control Allocation in Vehicle Dynamics Control for Rollover Mitigation", 2008 American Control Conferance, Washington, 2008
[22] O. haerkegard, "Backstepping and control allocation with applications to flight control", Ph.D. dissertation, Linkping University, 2003

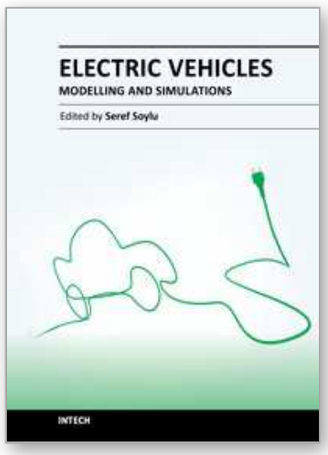

Electric Vehicles - Modelling and Simulations

Edited by Dr. Seref Soylu

ISBN 978-953-307-477-1
Hard cover, 466 pages
Publisher InTech
Published online 12, September, 2011
Published in print edition September, 2011

In this book, modeling and simulation of electric vehicles and their components have been emphasized chapter by chapter with valuable contribution of many researchers who work on both technical and regulatory sides of the field. Mathematical models for electrical vehicles and their components were introduced and merged together to make this book a guide for industry, academia and policy makers.

InTech Europe
University Campus STeP Ri
Slavka Krautzeka 83/A
51000 Rijeka, Croatia
Phone: +385 (51) 770 447
Fax: +385 (51) 686 166
www.intechopen.com

InTech China
Unit 405, Office Block, Hotel Equatorial Shanghai
No.65, Yan An Road (West), Shanghai, 200040, China
中国上海市延安西路65号上海国际贵都大饭店办公楼405单元
Phone: +86-21-62489820
Fax: +86-21-62489821

IntechOpen